Investigation of a High Voltage Hollow Cathode Electron Beam Source

Hansen, Johnny

Publication date:
1977

Document Version
Publisher's PDF, also known as Version of record

Risø Report No. 359

Risø Report No. 359

Risø National Laboratory

Investigation of a High Voltage Hollow Cathode Electron Beam Source

by Johnny Hansen

April 1977

Sales distributors: Jul. Gjellerup, Sølvgade 87, DK-1307 Copenhagen K, Denmark

Available on exchange from: Risø Library, Risø National Laboratory, DK-4000 Roskilde, Denmark

INIS descriptors

BREAKDOWN
COLD CATHODE TUBES
ELECTRIC POTENTIAL
ELECTRON BEAMS
ELECTRON GUNS
ELECTRON SOURCES
GLOW DISCHARGES
HOLLOW CATHODES
KEV RANGE 10-100
MEDIUM VACUUM
PASCHEN LAW
PLASMA INSTABILITY

UDC 537.533.2 : 621.385.1.032.212

April 1977 Risø Report No. 359

Investigation of a High Voltage Hollow Cathode Electron Beam Source

by

Johnny Hansen

Risø National Laboratory
Accelerator Department

Abstract

An investigation is presented of the possibility of developing an electron accelerator comprising several radiation units with a relatively low power per unit, and without the many elements such as accelerator tube, focusing and scanning systems. A study was desired of an electron gun operated at 200 kV based on the cold, hollow-cathode principle, where problems concentrated on the design of an electrode configuration that could withstand the high voltage at a pressure where a plasma could be generated too. Studies concentrated on the high voltage breakdown criterion in the pressure range 10^{-3} to 10^{-2} torr and on the plasma formation in a low pressure gas discharge.

Controlled beams with energies up to 130 keV were generated in nitrogen at a pressure of $2 \cdot 10^{-3}$ torr with a beam current of about 1 mA in a continuous operation. The high voltage was limited by the existing power supply in the laboratory; however, a decision was taken not to purchase a power supply that could have delivered the required voltage.

ISBN 87-550-0462-8

CONTENTS

1. INTRODUCTION

The utilization of ionizing radiation for industrial purposes has not expanded as rapidly as was anticipated fifteen years ago. At that time a considerable amount of fundamental and empirical knowledge had already been accumulated in the field of radiation chemistry, and it was possible to point out many types of processes, which technically as well as economically could be attractive for industry. Many circumstances contributed to delay this development, and it was generally believed when we started up the project under discussion that one of the more serious drawbacks was the lack of reliable, inexpensive radiation equipment.

The business of the accelerator companies has mostly been based on the design of advanced radiation equipment for scientific purposes, e.g. high energy accelerators for nuclear physics, and there has been insufficient economic incentive in developing radiation equipment for industry. As a consequence, companies interested in using ionizing radiation in production have been forced to make large financial investments in order to start these processes. In addition, the machines available have demanded a highly specialized staff of technicians as their construction has been complicated and, unfortunately, very unreliable.

The development of electron accelerators for industrial purposes has tended to be towards rather powerful machines, as the cost per unit power decreases with increasing power installed. This development is, of course, very natural but not very appropriate for introducing a new technique on a small scale, or for smaller companies. Another essential argument against the conventional machines, in which the electron beam is well-focused, scanned, and if necessary also pulsed, is that the dose rate, i.e. the absorbed energy per gram per unit time, is often too high in the material to be irradiated. This is, of course, more pronounced when using a more powerful machine. In certain processes a high dose rate not only introduces low ionizing radiation efficiency, but it could also seriously damage the surface to be treated, because of an excessive heat concentration.

We have therefore considered the possibility of developing

an electron accelerator consisting of several radiation units with a relatively low power per unit, and if possible without the many expensive elements such as accelerator tube, focusing and scanning systems. An optimum solution would be a continuous beam of electrons performing large-zone irradiation in the driving direction of the conveyer belt. A broad "beam-curtain" implies that the material to be irradiated, for a given total dose, remains longer in the radiation zone, thus resulting in an essentially smaller dose rate.

A broad "beam-curtain" could, e.g., be established by placing several electron guns, each with a relatively low power, beside each other. A set-up consisting of several electron guns might result in reasonable dose homogeneity, and at the same time make focusing and scanning systems unnecessary. Stability demands to the individual unit would be reduced, too. Grouping into several units also results in a higher degree of total reliability, as one or more individual units could fail simultaneously without seriously reducing the absorbed dose, or bringing the production line to a stop.

The design aim would be to achieve as simple and inexpensive a construction of the individual units as possible, where replacement procedures would be easy. If possible, construction should be so simple that, from an economical point of view, it would be cheaper to replace a damaged unit than to repair it, as is the case for electronic components such as klystrons and thyratrons.

The small accelerators, or electron guns, are envisaged connected to a single power supply having an output voltage corresponding to the desired electron energy. In this way, of course, the power supply would be decisive for reliability, but commercially available power supplies are very reliable for the voltage and power in question.

As it was our intention to design a machine superior to conventional low-energy electron accelerators in respect to price, reliability, and flexibility, new principles had to be considered. Based on the experience of Professor J. Silvermann at the University of Maryland, it was decided to start investigations of an electron gun based on the cold, hollow cathode principle. Some of the demands to a small accelerator are high current

intensity, soft vacuum and insensitivity to contamination. The cold cathode meets these requirements, and moreover has the advantages of high efficiency, relatively little heat development, no hot filament to be contaminated, self-focusing action, and primitive mechanical and electrical construction; as it operates in a soft vacuum, the use of high-vacuum equipment is eliminated. There are, of course, some drawbacks such as a high sensitivity to variations in pressure, difficulty in controlling the plasma at a high voltage level, and finally lack of knowledge of the limitations of the principle.

Controlled electron beams with energies up to 130 keV have been generated in nitrogen at a pressure of $2 \cdot 10^{-3}$ torr and with a beam current of about 1 mA in continuous operation. At lower voltages, current has been increased to 25 mA producing a beam with a current density of 0.75 A/cm^2. Power supply limits were 130 kV, 25 mA. Investigations have been made of diode-type plasma electron guns for operation at a high voltage level and with a fine collimated electron beam, beam diameter $\sim$ 2 mm, as well as of a triode-type electron gun producing a beam of 4 cm in diameter. In the triode type, the electron beam is accelerated, after extraction from the discharge plasma, to a high energy in a plasma-free region prior to passing through a thin metal foil window that is replaced in our experiments by a collector block. Power conversion efficiency has been measured to approx. 75%.

2. DESIGN OF THE COLD CATHODE ELECTRODE CONFIGURATION

From the initial investigations and measurements on smaller laboratory models, it was obvious that problems were mainly concentrated on the design of an electrode configuration that could withstand the high voltage without breakdown at a pressure where a plasma could be generated too. If it was possible to develop an electrode geometry able to withstand the high voltage requirements, then the basic idea in our philosophy of a simple, reliable, and inexpensive low energy electron source would be realised.

In the design of the cold-cathode plasma-gun, there are two contradictory interests from a high voltage point of view. In order that the electrodes can withstand a high voltage difference

without breakdown, a high vacuum would be desirable as the insulating dielectric. At the same time, however, the generation of a plasma from which the electrons are extracted calls for a rather soft vacuum. In the actual case, where the operating pressure is in the range 10^{-3} - 10^{-2} torr, the voltage breakdown criterion can be considered from two points of view, (i) the vacuum breakdown, (ii) and the Paschen breakdown.

2.1. Vacuum Breakdown

In the case of vacuum breakdown, many different hypotheses have been put forward in attempts to quantitatively explain the mechanism initiating electrical breakdown in vacuum in order to obtain more general experimental results. Great difficulty is experienced in deciding which of the large number of experimental results available should be used as a basis for the design data of equipment utilizing vacuum insulation, as the gaps used in various devices range from the order of millimetres to metres. The majority of the experimental results reported are conditioned values obtained under reasonably clean and controlled experimental conditions. Quite often it is the initial breakdown value that is of interest, but this value can be much smaller than the conditioned value. By a conditioned surface is understood a surface baked out in vacuum at high temperature, and where the microscopic irregularities originating from manufacture are removed by allowing a pre-breakdown current to flow in the gap for some time. Also most experimental results are for gaps of less than 1 cm, so extrapolation is required when estimating the electrical strength of longer gaps. Such extrapolation is dangerous because of the inability of the larger gaps to support electrical stresses (1) of the same order as the smaller gaps.

One empirical design criterion for the minimum sparking voltage of a vacuum gap is that put forward by Kilpatrick (2). This criterion is claimed to apply to the large range of surface gradients between $9 \cdot 10^6$ and $8 \cdot 10^9$ V/m, gaps up to 100 mm, and voltages up to $1.2 \cdot 10^6$ volt in the pressure range of 10^{-7} to 10^{-3} torr. Kilpatrick's work led to the expression:

$$V_s^3 \exp\left(-\frac{K_1}{V_s} d\right) = K_2 d^2$$

where V_s is the minimum sparking voltage, d is the electrode separation, $K_1 = 1.7 \cdot 10^7$ volt/m, and $K_2 = 1.8 \cdot 10^{18}$ volt^3/m^2. By iterative calculation, a curve is calculated showing the sparking voltage as a function of the electrode separation, fig.1.

Kilpatrick concluded that the criterion was valid for any metal electrodes, even if contaminated, and that it determined a threshold below which no breakdown should occur even before conditioning. The Kilpatrick criterion may be termed a pessimistic estimation, as the breakdown voltage must be higher for polished uncontaminated electrodes.

Cranberg (3) noted that there appeared to be a simple relationship between the gap length and the breakdown voltage of a plane-parallel vacuum gap. He showed theoretically that the relationship should take the form

$$V_s = K d^{\alpha}$$

where V_s is the breakdown voltage, K a constant, the value of which depends on the material and surface condition of the electrodes, d the gap length, and α the slope of the breakdown voltage-gap curve with a value of about 0.5 depending on the material.

Alpert et al. (4) showed by experiments a good agreement with Cranberg's theory for gap lengths of 10^{-6} m to 10^{-1} m, fig.2.

A more recent investigation by Lyman et al. (5) of the breakdown voltage of a plane-parallel vacuum gap showed that for gaps of less than about 1 mm in length, the breakdown voltage is approximately proportional to the length, all other parameters being kept constant. For such small gaps, the breakdown stress is relatively high, being of the order of $6 \cdot 10^7$ V/m. As the distance between a pair of plane-parallel electrodes in vacuum is increased beyond 1 mm, the breakdown voltage does not increase at an equal rate and so the breakdown stress for longer gaps is much reduced, being about $7 \cdot 10^6$ V/m at 10^{-1} m, fig. 3.

The vacuum breakdown is assumed to be valid as long as the mean free path of the molecules in the gas is larger than the gap length. For a pressure of 10^{-3} torr of nitrogen at room temperature, there are about $3.5 \cdot 10^{19}$ molecules/m^3 and the length of the mean free path (6) is about $5 \cdot 10^{-2}$ m, fig. 4.

2.2. Dielectric Breakdown

Near and to the right of the Paschen minimum the Townsend theory of pre-breakdown current growth is generally accepted to be valid (7). This theory is based on an equation with two basic coefficients, the primary ionization coefficient α, and the secondary ionization coefficient γ, which give the formula for current growth:

$$\frac{i}{i_o} = \frac{e^{\alpha d}}{1-\gamma(e^{\alpha d}-1)}$$

where i is the total current, i_o the initial photo-current, and d the gap spacing. The breakdown criterion is obtained by allowing $\frac{i}{i_o} \to \infty$, thus giving

$$\gamma(e^{\alpha d} - 1) = 1.$$

However, it is acknowledged that the Townsend theory cannot be used at low pressures and high voltage gradients, $\frac{E}{p} > 3 \cdot 10^5$ V/m torr, on the left branch of the Paschen curve up to the region of vacuum breakdown. This is because the electrons do not reach an equilibrium drift velocity in the gap, and a mean value for α cannot be defined.

It has been shown by Parker and Johnson (8) that there still exists an avalanche effect at a higher value of E/p. However, it is necessary to define a coefficient M, which is the total multiplication produced in the gap by each electron leaving the cathode including the contribution to ionizing collisions by electrons reflected back into the gas from the anode surface. They suggested a current growth equation

$$\frac{i}{i_o} = \frac{M}{1 - \gamma(M-1)}$$

which, for E/p values less than $4 \cdot 10^6$ V/m torr, provides good agreement with experimental results. The multiplication factor M takes the form of

$$M = \exp\left(\frac{pd}{V_o} \int_o^{V_o} q(V)dV\right)$$

where V_o is the applied voltage and q(V) the ionization cross-section of the gas. It is interesting that variation of either p or d has no effect on current growth if the pd product remains constant, i.e. the laws of similarity are obeyed in the region observed to the left of the Paschen minimum. The application of the similarity principle makes it possible to expand the usable voltage and pd-range of the experimental data obtained, as long as the calculation concerns conditions where the mean free paths of the charged particles or molecules are comparable to the distance between the electrodes.

As the multiplication factors for nitrogen in the voltage range of interest are not reported, values for some inert gases and steel electrodes are taken as basis for quite a good estimate. Figure 5 shows Paschen curves for some inert gases and steel electrodes that have measured sparking voltages up to 100 kV at a pressure of about 10^{-2} torr (9,10). At high voltages, however, the effect of ionization by electrons reflected from the anode surface back into the gas is of great importance, and use of an anode material with an electron reflection coefficient lower than that of steel will make the breakdown curve move towards a higher pd-value. The dependence of the secondary emission coefficient γ on gas and electrode material as a function of the applied voltage is rather complex, as the energy spectrum of the ions impinging on the cathode is difficult to determine. For kinetic electron emission with ion energies in the range of several kilovolts, γ increases with decreasing ion mass; but there are experimental data showing the reverse relationship. From the experimental breakdown voltage curves shown in fig. 5, it is obvious that a decrease in the total cross-section for ionization in inert gases leads to a successive increase in the breakdown voltage. As the total cross-section for the ionization of molecular nitrogen is a little lower than for argon, it is reasonable to use the argon breakdown voltage curve as an estimate for the nitrogen gas (11).

The reported experimental data show a voltage breakdown curve up to 100 kV. An extrapolation above this value is based upon the investigations reported in the literature and upon inspired guess-work.

2.3. Estimation of the Electric Stress

The basic investigations of the breakdown criteria have been discussed, and the results are shown in fig. 6 where the vacuum and the Paschen breakdown voltages are plotted as a function of the electrode gap separation.

It is obvious that there is a region between the two breakdown characteristics where high-voltage operation is possible without breakdown. The Cranberg and Lyman criteria are rather similar, and do not much differ in the gap length region of interest, whereas the Kilpatrick criterion is somewhat pessimistic. As the former criteria are based on experimental values and verified by other investigators, in contrast to the Kilpatrick criterion, which is based on a theoretical formula, there are good reasons to choose the more optimistic ones.

When comparing the vacuum breakdown with the Paschen breakdown criterion, the pressure must be kept sufficiently low to ensure that the gap length is comparable with the mean free path of the gas molecules. In this case, where the pressure is regarded as a soft vacuum, the vacuum breakdown curve as function of gap length must be very carefully considered.

At a pressure of 10^{-2} torr the distance between plane-parallel plates may vary from $5 \cdot 10^{-3}$ m to $5 \cdot 10^{-2}$ m at 200 kV without breakdown, and the respective electric field sizes will be from $4 \cdot 10^{7}$ to $4 \cdot 10^{6}$ Volt/m. Alpert et al. (4) showed that breakdown takes place at a constant effective cathode field of about 10^{9} V/m, when the electrode surfaces are smooth and clean and at room temperature.

Most of the experimental work has been carried out hitherto with electrodes giving a nearly uniform field in the gap, and the tendency has been to assume that the radius of curvature of the electrodes is without effect. However, Donaldson and Rabinowitz (12) showed that electrodes of the same materials, with the same surface finish, and using the same procedure, can have significantly different breakdown values due to the effect of electrode curvature. They found that more convex electrodes had higher breakdown field sizes and thus higher breakdown voltages than more nearly plane electrodes. With a sphere opposite a plane, the breakdown voltage increases as the diameter of the sphere decreases. For gaps of the order of 10^{-2} m and greater,

this effect starts reversing, i.e., the smaller the diameter of the sphere, the lower the breakdown voltage. However, even for large gaps this configuration still gives higher breakdown values than electrodes with a uniform field geometry.

This means that if the field stress is kept below the value adopted from the breakdown curve, then the actual concentric electrode geometry should not require a lower value in order to avoid breakdown.

When considering the electrode separation at a given voltage, here 200 kV, it is desirable to keep the operating point nearer to the vacuum breakdown characteristic, because this characteristic is expected to be more stable in time than the Paschen curve, which is sensitive to variations in pressure. Further, taking into account the possibility of building up an avalanche effect, it is worth keeping the electrode gap length close to the mean free path length of the nitrogen molecules at the operating pressure and temperature. Choosing a gap length of $1.5 \cdot 10^{-2}$ m allows the voltage in a plane to plane geometry to be almost double without incurring a vacuum breakdown, whereas the pressure may vary more than a factor of 4 before a Paschen breakdown occurs.

Finally, the electrode radius of curvature, influencing the field stress on the cathode surface, must be optimized. Most of the investigations on the high voltage breakdown criterion used in this work are performed with a plane-parallel electrode geometry, but in spite of the above mentioned work of Donaldson and Rabinowitz (12) it is advisable to keep the stress as low as possible.

In the present coaxial cylinder geometry, the voltage difference and electric field stress relationship is given by

$$E(r) = \frac{V}{r_1 \ln \frac{r_1}{r_2}}$$

where V is the applied voltage, r_1 and r_2 are the inner respectively the outer cylinder radius. By differentiation of E(r), the optimum ratio of the radii is found to be $r_2/r_1 = e$ giving the smallest overall dimensions for a given voltage and field stress. In fig. 7 the parameter $d = 1.5 \cdot 10^{-2}$ m shows that not

very much is gained in the V/E ratio by increasing the electrode radius. To keep the dimensions of the total electrode assembly within a practical size, the electrode radii are chosen as r_1 = 2.5 cm and r_2 = 4.0 cm, giving a V/E ratio of 1.2 and the corresponding field size of $1.7 \cdot 10^7$ volt/m for an applied voltage of 200 kV.

From theoretical investigations and experiments on the plasma in the region around the part of the anode and cathode that extend into the ionized gas of the positive column of the discharge, a correct electrode configuration was evaluated by a field-mapping technique using the NEUCC computer at the Technical University of Denmark. The computer program prepared by Jens F. Madsen, DtH, (27) calculates the potential distributions in a rotational symmetric static field of the Laplace type, i.e. conservative, static fields having contours and known potentials as boundary conditions. From the description of the physical configuration, the computer divides up the electrical field region by means of a mesh, from which is made an electrical analogue to the field problem. A calculation of the voltage at all grid points is performed and from these junction voltages, points on the equipotential lines of interest are calculated by interpolation. The computer gives the result of the calculation in a plot were the equipotential lines are drawn through the calculated points. The final plot is shown in fig. 8.

The electrode surfaces form the physical boundaries between which a voltage breakdown will take place, and so the breakdown strength depends on the electrode material. From a high voltage point of view, it is evident that stainless steel is superior to most other materials that could be used. In the present experiments a brass material was used. This is not very good compared to stainless steel, but has some advantages such as easy machining and good heat conduction. The rather complicated (at least from the point of view of machining, if made of brass) electrodes could be manufactured in our own workshop, which had some advantages, and the electrode configuration and geometry could just as well show if the design was appropriate. Further, use of good conducting material could render a cooling arrangement superfluous.

Before applying the high voltage to the gun, the electrodes were conditioned. After a bake-out at 200°C for four hours small

irregularities on the surface originating from the machining were burned off by means of a very weak glow discharge in pure nitrogen at a low voltage and at elevated pressure. The gun has been operated at $2 \cdot 10^{-3}$ torr and at a voltage of 130 kV, which is the highest potential our present power supply can yield.

3. DESIGN CRITERION OF THE COLD CATHODE

3.1. A Qualitative Explanation of the Hollow Cathode Operation

Very schematically, the cold, hollow-cathode electron-beam source consists of an insulated hollow metal cylinder, the cathode, containing an ionized plasma from which electrons are extracted through a small beam aperture, fig. 9. The cathode is surrounded by a grounded shield forming the anode. A high voltage is applied between the cathode and the shield, and with adequate gas pressure an abnormal glow discharge occurs (13). When a gas is admitted at 10^{-3} to 10^{-2} torr, a glowing plasma fills the interior of the cathode and a beam of electrons emerges from the cathode exit aperture into the vacuum chamber (14). The beam path is marked by the luminosity of gas atoms excited by collisions with electrons in the beam. Even though it has an output of several hundred watts (600 watt in a laboratory model), the uncooled cathode cylinder made of brass is relatively cold. From the colour of the cathode, the temperature is estimated to be 100-200°C. A typical current-voltage-pressure relationship at a low voltage level is shown in fig. 10. The output current dependence of the cathode aperture is shown in fig. 11.

The plasma electron-beam source operates when positive ions from the ionized gas outside the cathode are accelerated into the cavity by the high electric field near the cathode aperture (15). By ionizing collisions with the gas atoms present, and with the inner walls, an ionized body of plasma is formed inside the cathode cylinder. Surrounded by a space charge sheath, the cathode dark space, the internal plasma maintains itself at a potential that is positive with respect to the cathode, and negative with respect to the external plasma and the anode. Figure 12 shows a glow discharge between parallel

plates. It is seen how the major part of the anode to cathode voltage is located across the cathode dark space. In principle, the cylindrical geometry is similar to the parallel plate one. Figure 13 shows a photograph of the dark space and the glowing plasma inside the hollow cathode cavity. Electrons ejected from the internal walls by ion bombardment and by photoemission are accelerated across the sheath and decelerated in the plasma where they make ionizing collisions, further intensifying and maintaining the plasma. Due to the concentric shape of the cathode the majority of the reflected electrons pass through the centre area of the plasma column where a high density of electrons is formed. Losing most of their energy, some of the electrons move towards the increasing electric field at the cathode aperture and drift in the centre axis direction. Here they are focused by the electrostatic lens action of the aperture and accelerated by the very strong electric field in the external cathode dark space.

Because the gas pressure in the vacuum chamber is relatively low, only a few of the electrons in the beam collide with gas atoms, and therefore beam scattering is negligible. As positive ions are always present in the beam path,they attract electrons towards the beam axis and thus contribute to good beam collimation in the vacuum chamber (16). This gas-focusing phenomenon accounts for the long self-focused beam that is characteristic of the plasma electron-beam source.

The beam current may be continuously controlled by varying either the gas pressure or the high voltage to the cathode. A control grid mounted inside the cathode cylinder may also control the beam current. This grid consists of a mesh cylinder of fine stainless steel wire open at the down-stream end and supported from a coaxial stem insulated from the cathode tube. The transmission of the mesh is about 25%. With a floating grid, the grid potential will assume the internal plasma potential positive with respect to the cathode. A variable resistor connected between the grid and the cathode makes a simple regulation of the internal charge density by regulating the positive ions to the cathode walls and repelling the secondary electrons, and thus controlling the electron beam current (fig. 14).

The electron gun aperture is located at the down-stream end of the chamber. This aperture may be a very thin titanium or aluminum foil window, or a differentially pumped conduit from which the electrons emerge into the air. In the laboratory model, this aperture is replaced by a target mounted inside the vacuum chamber from where the electron beam current is measured.

3.2. Investigations of the Hollow Cathode

In our work on the development of a high-voltage electron-gun we found it important to determine the optimum geometry (e.g. cathode diameter) able to emit a suitable, controlled electron current, and at the same time able to support the high voltage for acceleration of the electrons to the desired energy. For this purpose, an investigation was made of hollow-cathode performance and a brief study of the literature.

The theory of low-pressure glow discharge indicates that in the discharge most of the applied cathode-to-anode voltage is required for the cathode dark space, and that the negative glow and the Faraday dark space are essential to the discharge, whereas the positive column could be avoided. As the gas pressure is reduced, the negative glow and the Faraday dark space appear to expand until at a sufficiently low pressure first the Faraday dark space and finally the negative glow disappear. When the Faraday dark space has disappeared, probe measurements showed that the plasma in the negative glow assumes a potential a few volts more positive than the anode. When the negative glow disappears, the discharge current vanishes. This indicates that the phenomena at and near the cathode are essential to the discharge, and that the positive column merely serves to maintain a conducting path for the current. Figure 12 gives a picture of the formation of a glow discharge between parallel plates; this formation will be the same in the hollow cathode situation if one imagines that the picture is reflected on the cathode centre axis.

Just at the cathode there is a small net negative charge produced by the electrons being emitted. As the electron current density at the cathode is relatively small, the current is carried almost entirely by positive ions arriving at the cathode from the cathode dark space. The dark space is therefore a region of

high positive ion density (17). This charge distribution produces the large potential drop in the cathode dark space. In the negative glow the electron concentration increases to such an extent that the net charge density is nearly zero and the potential reaches a maximum value with a low electric field. From probe measurements, the electron concentration may be as high as 10^{12} parts per cm^3. In the Faraday dark space the field again increases and the field gradient near the negative glow side may actually become negative, as seen from measurements on the plasma where the plasma is found to be almost at the anode potential.

Determinations of the field distribution in the cathode dark space for a plane parallel geometry indicate that a linear relation is essentially correct, although there may be deviations at both the cathode and the negative glow side. If the field distribution in the entire cathode dark space is assumed to be linear, a relation between the potential drop, the current density and the cathode dark space thickness can be evaluated by means of the Child-Langmuir space-charge equation. But in the case of a cylindrical geometry, where the field distribution in the dark space is not linear, a correction factor β^2 must be added. From fig. 12 it is seen that a positive charge density dominates in the entire cathode dark space; this is because of the relatively high mobility of the electrons. Therefore it is relevant to calculate on the ion current density in the space charge equation and to regard the cylindrical plasma column as the ion-emitting electrode. The Child-Langmuir space charge equation now takes the form of

$$i^+ = \frac{4\varepsilon_o V^{3/2}}{9 r^2 \beta^2} \sqrt{\frac{2e}{M}}$$

where ε_o is the free space permittivity, e is the electron charge, M is the ion mass, and V is the voltage. β^2 is a function of the ratio $\frac{r}{r_o}$, where r is the cathode cylinder inner radius, r_o is the radius of the emitting plasma cylinder, and so $s = r - r_o$ is the dark space thickness. This equation has been verified by experiments covering a wide range of conditions, and it is valid for any electrode, even a cold one, that permits electrons or ions to escape from it (18).

From investigations in our laboratory this equation seems to be valid for the current density in the normal glow discharge; but in order to increase the current from the plasma, the cathode is operated in the abnormal glow discharge mode. Here the cathode dark space voltage-difference and the current density increase, whereas the cathode dark space thickness decreases. Engel and Steenbeck (19) have shown that when the cathode dark space voltage-difference increases, and the ratio of abnormal to normal current density exceeds a value of about 20, the cathode dark space thickness converges towards a value of 0.4 times the value at a normal glow discharge. Thus the dark space thickness is calculated under normal glow discharge conditions and then multiplied by the factor mentioned above.

$$r^2\beta^2 = 0.4 \frac{4\epsilon_o V^{3/2}}{9 i^+} \sqrt{\frac{2e}{M}}$$

However, the similarity principle is no longer valid for an abnormal glow discharge in a cylindrical geometry, because the cathode dark space thickness is found to be unchanged within a pressure variation of a factor of more than 10. As the current density at the cathode of the abnormal glow discharge may be quite high, there is always the possibility of heat developing there. This heat development may cause experimental values to vary owing to the emission properties of the cathode material and to changes in gas density near the cathode. These phenomena are most pronounced in the concentric type of cathode, because the interior of the hollow cathode cylinder is evacuated through the small orifice having a relatively low pumping speed.

3.3. Investigations of the Plasma Instability

Paschen (20) was the first to point out that cathodic processes depend on the geometry of the cathode. Through experiments with a discharge tube having a pair of parallel cathodes, he found that when their separation was reduced until it was comparable with the double of the cathode dark space, the discharge current increased by several orders of magnitude. The same results were obtainable with a hollow cathode in a cylindrical geometry and the phenomena is known as the double- or

hollow-cathode effect. The hollow-cathode effect appears and develops in an abnormal glow discharge when a certain relation is satisfied between the parameters such as pressure, diameter of the cylinder, cathode-fall voltage, and current density at the cathode.

Tonks and Langmuir (21) studied a low pressure mercury discharge maintained by a hot filament cathode and detected oscillations over a range of frequencies up to the plasma electron frequency. Popovici et al. (22) proposed that the amplification of the discharge current is due to an interaction between fast primary electrons accelerated in the cathode fall and slowly moving electrons of the plasma. This interaction results in a transfer of energy and should result in a strong increase in the density of the electrons that are able to excite and ionize. Niell and Emeleus (23) found that oscillations mainly occurred in a thin layer of plasma at the cathode sheath boundary. More recently, Lloyd (24) found, in a plane parallel hollow-cathode geometry, that the fast secondary electrons may be repeatedly reflected between the electrodes, thus further enhancing the transfer of energy to the plasma oscillation.

Several workers (21-24) have studied this effect at pressures from 0.1 mtorr to 10 torr, and one conclusion was that the hollow-cathode effect is in fact many effects, different aspects being important at different pressures and in varying geometries. Investigations have shown, however, that under nearly all conditions when a discharge is present, a potential well is formed inside the hollow cathode by a plasma near the anode potential, see fig. 15, and that the expression (1) for the cathode dark space region with correction for the abnormal glow mode is valid for the self sustained hollow-cathode discharge.

The theory proposed by Popovici and Lloyd for the hollow-cathode effect might to a good approximation be fitted to our experiments. In fig. 15 the plasma distribution, potential distribution and particle currents are shown schematically. In the abnormal glow discharge, as well as in the hollow cathode effect regime, most of the excitation and ionization processes occur in the negative glow plasma. Taking this into account, it is reasonable to consider the negative glow of the hollow cathode discharge as a plasma through which electrons are travelling

accelerated in the two cathode dark space sheaths. The origin of these electrons is a space-charge-limited current of ions falling through the sheath region from the plasma to the cathode ejecting secondary electrons, which are accelerated to a velocity corresponding to the sheath voltage drop. As the mean free path of these fast electrons is fairly large, most of them will penetrate the plasma and be reflected by the field in the sheath surrounding the plasma. Thus, oscillating back and forth, they lose their energy by collisions with neutrals and electrons in the plasma, or by other processes. In this way they contribute to an increase of transferred energy to the resonant plasma oscillations.

Studies on the electron velocity distribution in the negative glow plasma of the abnormal glow discharge (22) have shown a Maxwellian-like shape (full line in fig. 15c) with most velocities below a few electron volts, and a very small number of electrons, which are fast secondaries from the sheath, with velocities far above the ionization energy of the gas. The Maxwellian component is denoted "plasma electrons". The fast electrons can lose energy by, for instance, ionization processes, but also by plasma resonance oscillations. In the latter case some of the slowly moving plasma electrons or background electrons gain energy from the oscillation, and their velocity distribution will be levelled out resulting in a flatter distribution containing more particles in the domain of the ionization energy (dotted line in fig. 15c). In the plasma region, the electron plasma frequency is given by the usual expressions, and the transit time t_{ep} of the fast moving electrons through the plasma should approximate the electron plasma frequency ω_{ep}.

This resonant excitation of oscillations is essentially due to a two-stream type of plasma instability present in the plasma penetrated by a fast beam of charged particles. In this case we may consider the secondary electrons as a beam traversing the plasma with a velocity corresponding to the sheath voltage. The spread in this high velocity will be small, as illustrated in fig. 15c, so we may consider the beam as essentially having zero temperature. As the beam velocity is much larger than the thermal velocity of the background plasma, we may also neglect the thermal spread of this component. A detailed investigation

of this instability (25) shows that waves with wavenumber k in the range

$$0 \leq k \leq \frac{\omega_{ep}}{v_{es}} \left(1 + \sqrt[3]{\frac{n_{es}}{n_e}}\right)^{3/2}$$

are unstable. Here ω_{ep} is the plasma frequency of the background plasma, v_{es} the beam velocity and n_{es} and n_e the electron density of the beam and background plasma, respectively. It can be shown (25) that the most unstable oscillation is that with frequency $\omega = \omega_{ep}$, having a growth rate $\gamma = \frac{\sqrt{3}}{2} \omega_{ep} \sqrt[3]{\frac{n_{es}}{2n_e}}$ and a corresponding wave number $k_m = \omega_{ep}/v_{es}$. The growth rate as a function of k is sharply peaked around this value, fig. 16, and we shall therefore only consider the most unstable oscillation. Though the beam density is rather small, the instability is fairly violent, e.g. for $n_{es} \sim 10^{-3} n_e$ the growth rate $\gamma \sim 0.1\ \omega_{ep}$. For small beam densities, n_{es}, the instability may be understood as a resonant excitation of the natural oscillation of the background plasma, and the simplified expressions of Lloyd (24) are applicable.

When the thermal spread of beam and backgrcund plasma is no longer negligible, we may still have an unstable situation, but now it is merely a "bump on tail" type of instability with a diminished growth rate where the exact form of the velocity distribution is important. This situation is considered by Popovici (22), but since we are concerned with high values of sheath voltage drop, we shall not discuss this problem.

As mentioned above, we expect the density of the fast electrons to be small from the following argument: Because the ions are accelerated towards the cathode, flux conservation implies that their density n_i at the cathode surface is much smaller than the density n_e in the plasma. The secondary electron density n_{ec} at the cathode will then, at most, be of the order of n_i, as it is probable that the secondary emission coefficient $\gamma \sim 1$. These secondary electrons will be accelerated towards the plasma, and here again flux conservation implies a decrease in density when they reach the plasma, which means $n_{es} << n_i << n_e$ where n_{es} is the density of the fast electrons when entering the plasma. No contributions from electrons generated by ionizations in the dark space are expected to influence our conclusion, i.e. the beam electron density is small.

The above description applies to a hollow cathode in a plane parallel geometry such as that considered by Lloyd and Popovici, where two beams are involved, namely one originating from each sheath. As a good estimate, we may, however, apply the result to the cylindrical geometry.

In order to show a typical instability evolution, fig. 17a and b represents the hollow-cathode effect in current to voltage coordinates for a discharge in nitrogen at different pressures and with different cathode diameters. The current is the beam current from the cathode to the anode. The increase of current at a critical cathode voltage emphasizes the appearance of a new ionization process, which corresponds to the plasma instability. One might expect a steep rise and fall of current for increasing voltage, as in common resonance phenomena. One reason why this does not occur is that when the high density of charged particles is once established, it continues to exist as long as sufficient energy is fed into the system. Some of the waves with smaller growth rates may also play a role in this situation. There may be a very little decrease in current when passing the resonance condition, but this does not appear from the rather rough experimental readings.

3.4. Calculations of the Plasma and Sheath Formation

From the above investigations and considerations, an attempt was made to derive a set of equations that could lead to a design criterion for a concentric type of hollow cathode with optimum dimensions, also taking the high voltage considerations into account. It must be emphasized again, however, that the effect discussed here is probably only one of many contributions to what is called the hollow-cathode effect, but it may be the most important for our conditions. An example shows that the theory outlined is valid at least for lower voltages.

As shown in fig. 15, the internal diameter of the hollow cathode is divided into three regions, which are two dark space sheaths and a plasma region. The total transit time spent for an electron in traversing this distance may be expressed as

$$t_{total} = t_{ep}(\text{plasma}) + 2\, t_{es}(\text{sheath}).$$

For plasma oscillations with the dispersion resolution

$$\omega = \omega_{ep} \sqrt{1 + 3(kL_D)^2}$$

where $k = 2\pi/\lambda$, $\omega = 2\pi f_e$ and L_D is the Debye length, we find for $(kL_D)^2 << 1$ that $\omega \simeq \omega_{ep}$ is practically independent of the wave-number k. Then, as mentioned above, the transit time for a fast-moving electron to traverse the plasma region roughly corresponds to the range of the electron plasma frequency ω_{ep}, which means

$$\omega_{ep} = \sqrt{\frac{n_e e^2}{\varepsilon_o m_e}} \simeq \frac{2\pi}{t_{ep}} \quad . \tag{2}$$

Here n_e is the electron plasma density and m_e is the mass of the electron. The time t_{ep} might also be expressed by the internal cathode diameter d, the dark space thickness s, and the electron velocity in the plasma

$$t_{ep} = \frac{d - 2s}{v_{ep}} \quad .$$

The electron velocity in the plasma is to a good approximation the velocity when entering the plasma, which means $v_{ep} \simeq v_{es}$

$$e(V_{plasma} - V_{cathode}) = \tfrac{1}{2} m_e v_{es}^2$$

where

$$v_{ep} \simeq v_{es} = \sqrt{\frac{2Ve}{m_e}} \tag{3}$$

and so

$$t_{ep} = (d-2s) \left(\frac{2Ve}{m_e}\right)^{-\frac{1}{2}} \quad .$$

Here V is the plasma to cathode voltage difference, or approximately the cathode potential. From equations (2) and (3) an expression is now found for the length of the plasma region

$$2r_o = d-2s = t_{ep} v_{ep} = \frac{2\pi}{\omega_{ep}} \sqrt{\frac{2Ve}{m_e}}$$

and then the cathode inner diameter

$$d = \frac{2\pi}{\omega_{ep}} \sqrt{\frac{2Ve}{m_e}} + 2s \qquad (4)$$

where the sheath thickness s is calculated from equation (1). However, the sheath thickness $s = r - r_o$ is not found directly but expressed in terms of $r^2\beta^2$, where β^2 is a function of $\frac{r}{r_o}$. This relation is indicated in fig. 18, and the cathode radius r is evaluated by iterative approximations.

Expression (4) is valid as an estimate for any cold hollow cathode containing an abnormal glow discharge, but when searching for the above mentioned hollow-cathode effect, the radius r_o of the plasma region must attain a certain value. This value is determined by the plasma frequency ω_{ep} in such a way that the plasma region $2 r_o$ only has the extent of an even number of half wavelengths at the most unstable electron oscillation, $2 r_o = K\frac{1}{2}\lambda_{ep}$, with λ_{ep} being the wavelength of the oscillation; K is an integer. The equation expressing the optimal inner cathode diameter and leading to the hollow-cathode effect now takes the simple form

$$d = K\tfrac{1}{2}\lambda_{ep} + 2s \ . \qquad (5)$$

As an example of the validity of the theory outlined here, experimental results from a hollow cathode operated at a voltage level of about 2 kV give good agreement. The cathode is that shown in fig. 13, where the bottom plate with the beam aperture is replaced by a mesh that allows observation of the inside of the cathode while in use without disturbing the operation. The cathode cylinder and the solid shield supporting the mesh grid are in fact designed to operate with a low voltage difference. For higher electron beam energies, this system is then elevated to a high extraction voltage level above ground potential.

From a scale mounted on the glass of the viewing port, the plasma region, which is the glowing part, is found to have an extension of about 25 mm in a cathode cylinder of 40 mm in diameter. With a cathode voltage of 1850 volt and a beam current of 10 mA, Langmuir probe measurements show a plasma electron tem-

perature of 5.8 eV with an ion current I^+ to the probe of 2 μA, fig. 19. The electron and ion density in the plasma is calculated from

$$I^+ = n^+ e A \bar{v}^+$$

where $A = 3 \cdot 10^{-7}$ m^2 is the effective probe area and $\bar{v}^+$ is the mean ion velocity. It is assumed that the ion density equals the electron density, fig. 12, and that the mean ion velocity corresponds to the electron temperature rather than the ion temperature, the Bohm criterion (26).

$$\bar{v}^+ = \sqrt{\frac{2\kappa T_e}{M}} = 6.4 \cdot 10^3 \quad [ms^{-1}]$$

$$n_e \simeq n^+ = \frac{I^+}{eA\bar{v}^+} = 6.5 \cdot 10^{15} \quad [m^{-3}]$$

κ is the Boltzmann constant and M is the weight of a nitrogen atom.

From the plasma electron frequency ω_{ep}, the wavelength λ_{ep} of the plasma electron oscillation is calculated. Thus, use of the fundamental of the oscillation gives the minimum thickness of the plasma column.

$$\omega_{ep} = \sqrt{\frac{n_e e^2}{\varepsilon_o m_e}} = 4.6 \cdot 10^9 \quad [s^{-1}]$$

$$\lambda_{max} = \frac{4\pi}{\sqrt{3}\omega_{ep}} \sqrt{\frac{2Ve}{m_e}} = 4 \cdot 10^{-2} \quad [m]$$

plasma thickness: $2 r_o = K\frac{1}{2}\lambda_{max} = 2 \cdot 10^{-2}$ (m) for K = 1. A factor of $\frac{2}{\sqrt{3}}$ is added to the expression for λ_{ep}, resulting in the wavelength for the most unstable oscillation.

A calculated plasma thickness of 20 mm corresponds very well to the observed thickness of 25 mm, see fig. 13, especially as the plasma to sheath edge is not a well defined point, but rather consists of a transition area a few millimeters in length.

The dark space thickness is calculated from equation (1) and from knowledge of the ion concentration and velocity at the plasma-sheath edge. However, equation (1) does not give the sheath thickness directly, but as a function of the plasma thickness. The sheath thickness is found by means of the calculated radius r_o of the plasma column and by iterative calculations using equation (1) and fig. 18.

$$r^2\beta^2 = 0.4 \frac{4\ \varepsilon_o\ V^{3/2}}{9 n^+ e \bar{v}^+} \sqrt{\frac{2e}{M}} = 6.8 \cdot 10^{-5} \quad [m^2]$$

for $n^+ = 6.5 \cdot 10^{15}\ m^{-3}$, $\bar{v}^+ = 6.4 \cdot 10^3\ ms^{-1}$, and V = 1850 volt. In the actual case $r = 2 \cdot 10^{-2}$ m and

$$\beta^2 = \frac{r^2\beta^2}{r^2} = 0.17 \rightarrow r_o = \frac{r}{1.6} = 1.25 \cdot 10^{-2} \quad [m]$$

and finally the sheath thickness

$$s = r - r_o = 0.75 \cdot 10^{-2} \quad [m]$$

which is very close to the observed sheath thickness (fig. 13) of 7-8 mm.

The optimum diameter of the hollow cathode can be calculated by means of the theory outlined here. With knowledge of the sheath thickness, it is possible to correctly position an internal coaxial grid, thus providing control of the current intensity from the internal plasma to the cathode wall and hence a control of the electron beam current to the anode.

For increasing voltage, other parameters kept constant, the plasma wavelength will increase, and hence the thickness of the plasma column for optimum conditions. This means that the dimensions of the apparatus soon get very large. Figures 20, 21, and 22 show the plasma electron velocity, plasma frequency, and plasma oscillation wavelength, respectively, and fig. 23 shows the plasma thickness leading to the hollow-cathode effect as a function of the plasma to cathode voltage difference. With plasma diameters smaller than this critical wavelength, unstable oscillations can no longer exist in the plasma. Oscillations taking place at a higher wave number may probably exist, but

they will still decrease in amplitude with increasing wave number because of the damping of the higher frequencies. This damping becomes appreciable for wave numbers of the order of the Debye wave number, $k_D = \omega_{ep}/v_e$ (v_e is the root mean square thermal velocity of the electrons), or in other words the organized motion of plasma oscillations cannot be sustained for wavelengths shorter than about 10 times the Debye wavelength given by

$$L_D = \sqrt{\frac{\varepsilon_o \kappa T_e}{e^2 n_e}}$$

which is the distance over which small variations of potential vanish in a uniform material. T_e is the plasma electron temperature in degrees Kelvin. In the actual case, L_D is of the order of 10^{-4} m.

For other non-resonance conditions, there will be a plasma and a current flow but as mentioned earlier in this paper the presence of the negative glow and the Faraday dark space is essential for the glow discharge to take place. This means in practice that as long as the cathode diameter is able to contain two sheath thicknesses, there will be conditions for a discharge current to flow, but the resonance conditions are not strongly outweighted.

As the plasma to cathode voltage difference is increased and other parameters kept constant, the sheath thickness will increase, too. For voltages above 10 kV, it is relevant to estimate the plasma thickness to be of the order of ten times the Debye length if the cathode dimensions are to be kept practical. For a given current flow, the ion-current density i^+ can be calculated at the plasma-sheath transition edge, and thus the sheath thickness and overall cathode tube dimension. Figure 24 shows the calculated sheath thickness for a current flow of 100 mA.

In the actual cathode, which is designed to a diameter of $4 \cdot 10^{-2}$ m, experiments have shown that at 130 kV it is still possible to draw a current of a few milliamperes. This means either that a tiny plasma exists and so a very high current density, because of a small plasma surface, or that the current from the cathode consists directly of secondary electrons or cathode fragments from sputtering at the inner cathode walls.

In the above discussions and calculations the length of the

cathode cylinder has not been taken into account, but its influence was evaluated by some easily performable measurements. These investigations on a cathode at 20 kV having an internal cavity of variable length showed that a cylinder length of about 10 times the cylinder radius gave the best efficiency. In fig. 25 the power supply current and electron beam current are shown as a function of the cylinder length to diameter ratio. It is assumed that the relatively high current for a small ratio is due to a sputter of secondaries from the cylinder bottom plate caused by high energy ions entering the cavity through the cathode orifice. Under these conditions the cathode got rather hot, and as seen from the figure the efficiency also decreases compared to optimum conditions.

4. CONCLUSION

The cold cathode electron gun concept was investigated particularly with a view to a simple, inexpensive technique for generating electron beams specially suited for the processing of foils and surface coatings. As many of the earlier attempts to use this technique have been based on empirical methodes, and there are few measured properties, a more quantitative understanding of the relationship between voltage, current, electrode configuration, and discharge geometry has been attempted.

Experience indicates that beam power of the order of one kilowatt at beam energies of 10^5 electron volts is possible in a gas atmosphere of one to ten microns.

One feature of the hollow cathode concept to be emphasized is the possibility of generating a large-area electron beam with a relatively high current density and energy. For surface treatment, cross-. nking, and paint curing, a curtain-like electron beam can be generated, as well as specially shaped beams for, e.g., radiation processing of cable insulation, although the stability of such a "curtain" is not yet investigated.

ACKNOWLEDGMENTS

It is a pleasure to thank P. Lausen, Electric Power Engineering Department, the Technical University of Denmark, for helpful guidance in the computer calculations of the electrical

field region; F. Øster and H. Pécseli, Plasma Physics Group, Risø, for stimulating discussions and helpful suggestions concerning the plasma investigations; and M. Wille, Accelerator Department, for skilled assistance in building and testing the electron guns.

REFERENCES

1. Alston, L.L. (ed), High-Voltage Technology. (Oxford University Press, London, 1968) 408 pp.
2. Kilpatrick, W.D., Rev. Sci. Instrum. 28 (1957) 824-826.
3. Cranberg, L., J. Appl. Phys. 23 (1952) 518-522.
4. Alpert, D., Lee, D.A., Lyman, E.M., and Tomaschke, H.E., J. Vac. Sci. Technol. 1 (1964) 35-50.
5. Lyman, E.M. et al., In: Co-ordinated Science Laboratory. University of Illinois, Progress Report, June-August (1962) p.72.
6. Dushman, S., Scientific Foundations of Vacuum Technique. Chapter I. (Wiley, New York, 1962).
7. Cobine, J.D., Gaseous Conductors. Theory and Engineering Applications. (Dover, New York, 1958) 143-204.
8. Parker, A.B., Johnson, P.C., The Dielectric Breakdown of Low Density Gases, I and II. Proc. R. Soc. Lond. A. 325 (1971) 511-541.
9. Guseva, L.G., "Left-hand Branch of the Paschen Curve in Inert Gases up to 100 kV". Sov.-Phys. Tech. Phys. 15 (1971) 1760-1762.
10. Pace, J.D., Parker, A.B., The Breakdown of Argon at Low Pressure. J. Phys. D. 6 (1973) 1525-1536.
11. Hasted, I.B., Physics of Atomic Collisions. 2nd ed. (Elsevier, New York, 1971) 385-422.
12. Donaldson, E.E. and Rabinowitz, M., J. Appl. Phys. 36 (1965) 1314-1319.
13. von Engel, A., Ionized Gases. (Clarendon Press, Oxford, 1955) 281 pp.
14. van Paassen, H.L.L., Muly, E.C., Allen, R.J., Electron Beam Phenomena Associated with Perforated Wall Hollow Cathode Discharges. Proc. Nat. Electron Conf. 18 (1962) 590-596.
15. Boring, K.L., Stauffer, L.H., A New non-Thermionic Electron Gun. Proc. Nat. Electron Conf. 19 (1963) 535-544.

16. Linder, E.G., Hernquist, K.G., Space-charge Effects in Electron Beams and their Reduction by Positive Ion Trapping. J. Appl. Phys. 21 (1950) 1088-1097.

17. Cobine, J.D., Gaseous Conductors-Theory and Engineering Applications. (Dover, New York, 1958) 205-289.

18. Langmuir, J., Compton, K.T., Electrical Discharges in Gases. Rev. Mod. Phys. 3 (1931) 191-257.

19. von Engel, A., Steenbeck, M., "Elektrische Gasentladungen, ihre Physik und Technik". Vol. 2. (Springer, Berlin, 1933) p. 77.

20. Paschen, F., Ann. Phys. 50 (1916) 901-940.

21. Tonks, L. and Langmuir, I., Phys. Rev. 33 (1929) 195-210.

22. Popovici, C., Somesan, M., and Nistor, V., On the Hollow Cathode Mechanism. Ann. Phys. 19 (7. Folge) (1967) 225-233.

23. Neill, T.R. and Emeleus, K.G., Proc. R. Ir. Acad. Sect. A 53 (1951) 197-222.

24. Lloyd, O., Beam-Plasma Interactions in a Hollow Cathode. J. Phys. D 4 (1971) 1291-1301.

25. Briggs, R.J., Two-Stream Instabilities. Adv. Plasma Phys. 4 (1971) 43-78.

26. Bohm, D., Minimum Ionic Kinetic Energy for a Stable Sheath. In: The Characteristics of Electrical Discharges in Magnetic Fields. Edited by A. Guthrie and R.K. Walkerling. (McGraw-Hill, New York, 1949) 77-86.

27. Madsen, J.F., Om beregning af stationære felter ved elektriske netværksanalogier. (DtH, Stærkstrømsafdelingen, København, 1973). (Publ. no. 7307).

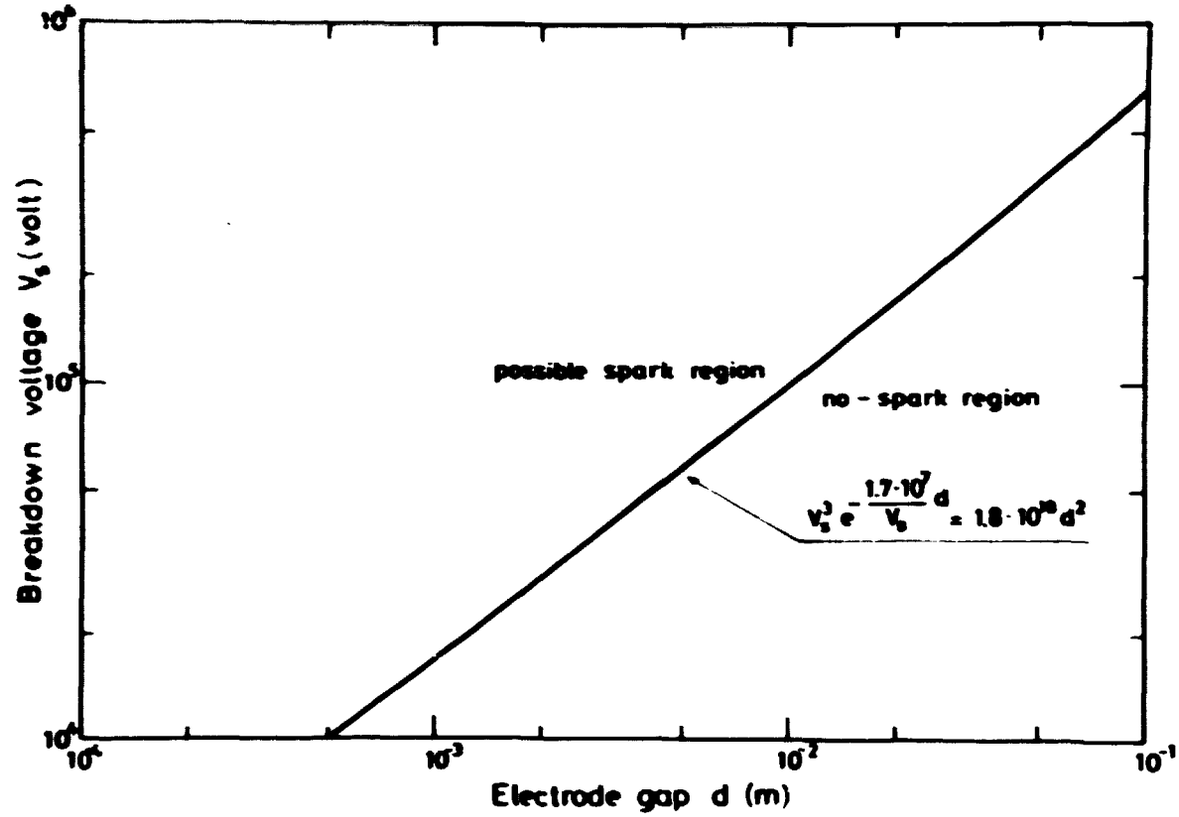

Fig. 1. Vacuum breakdown voltage, $10^{-7} < p < 10^{-3}$ torr, (Kilpatrick).

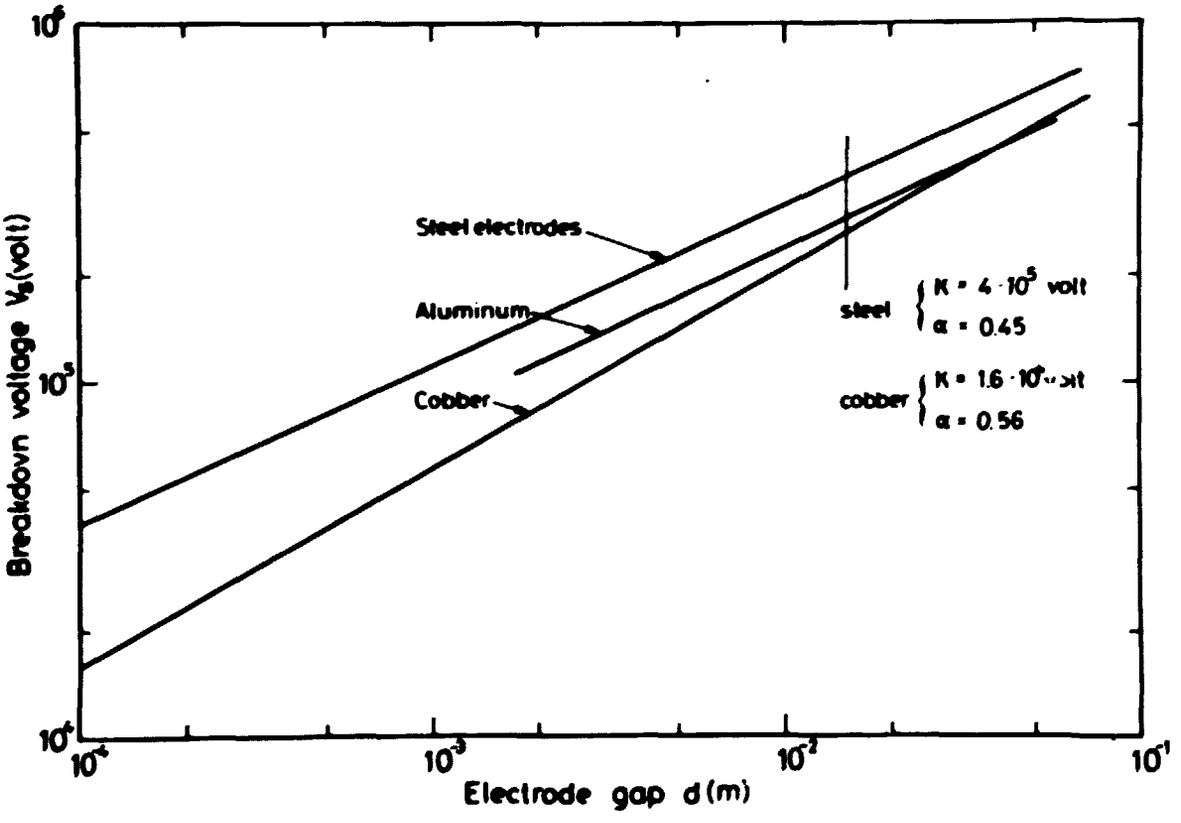

Fig. 2. Vacuum breakdown voltage, experimental, (Cranberg et al.).

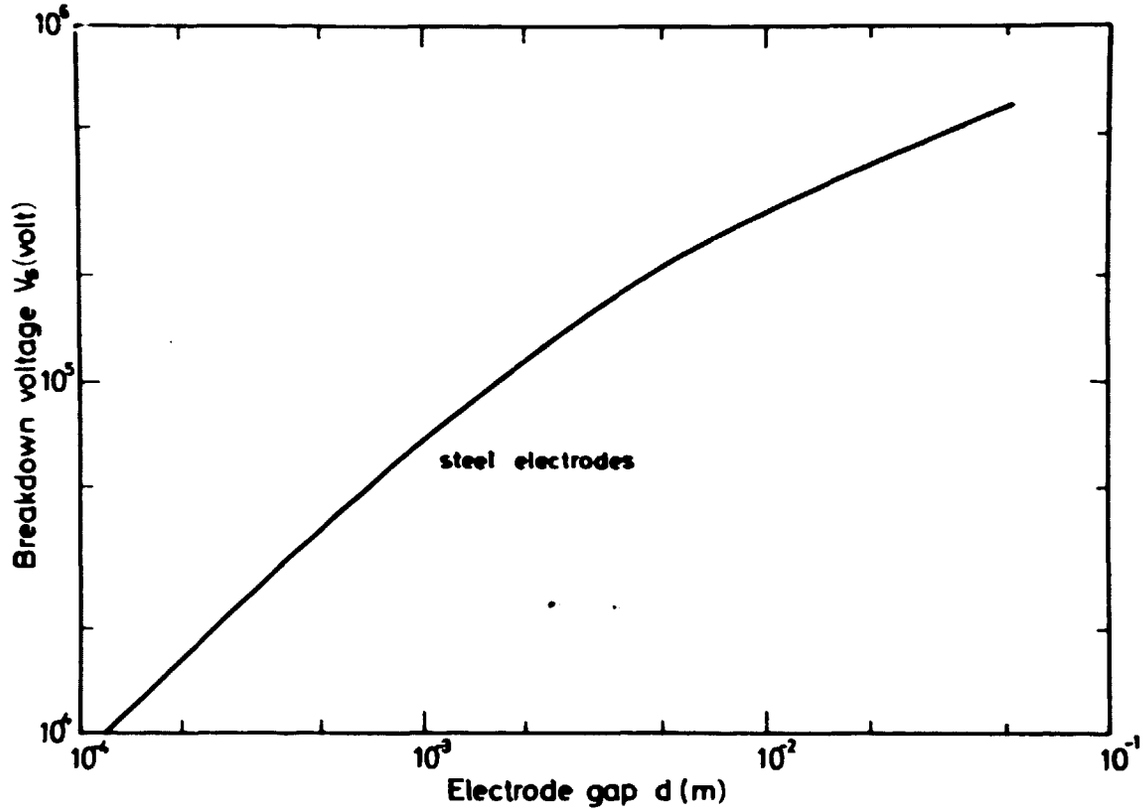

Fig. 3. Vacuum breakdown voltage, (Lyman et al.).

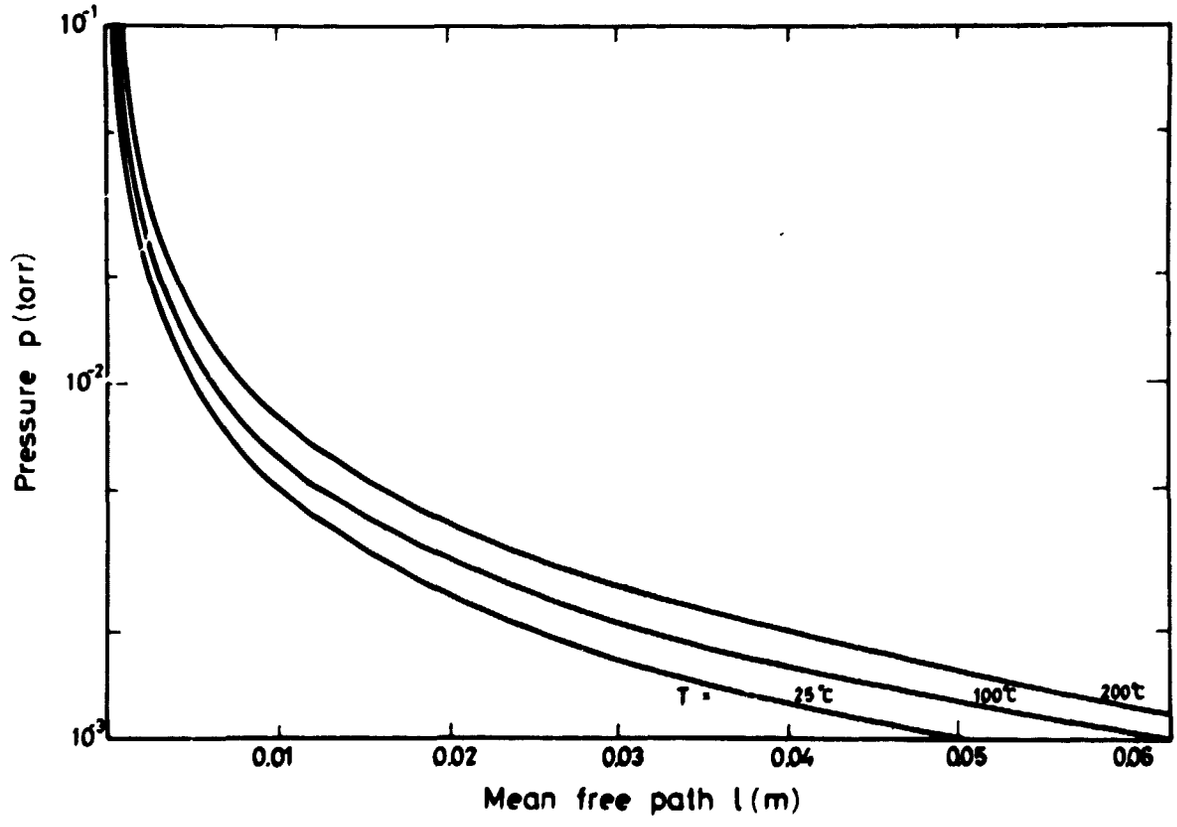

Fig. 4. Molecular mean free path in air, (Duschman).

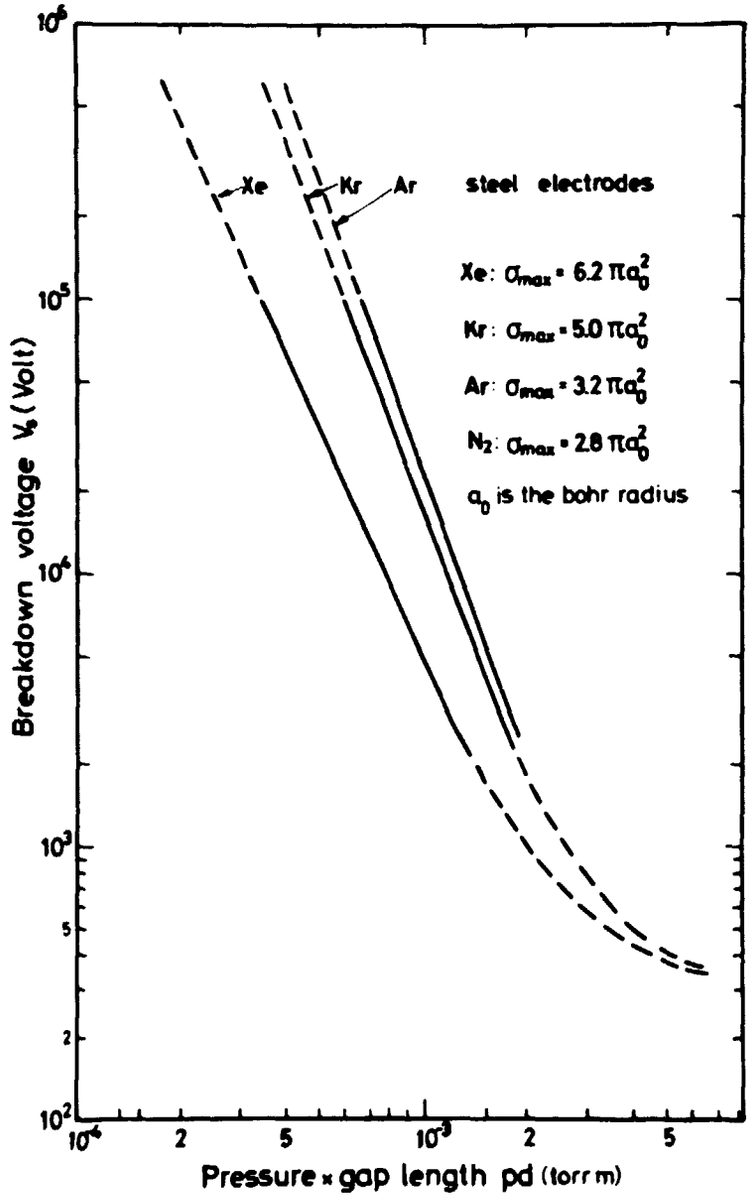

Fig. 5. Paschen breakdown voltage curve, (L.G. Guseva).

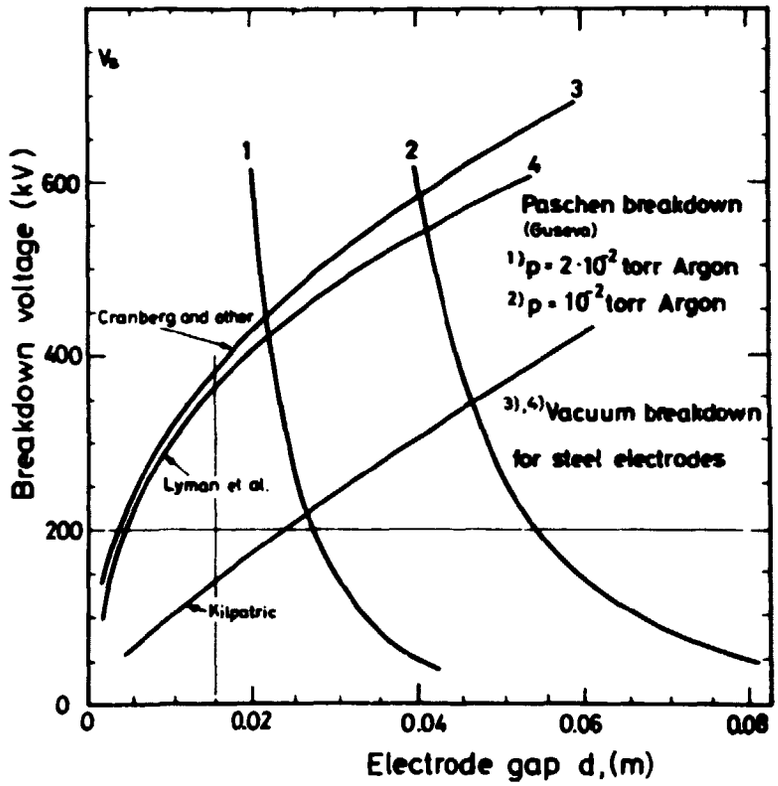

Fig. 6. Breakdown voltage characteristics.

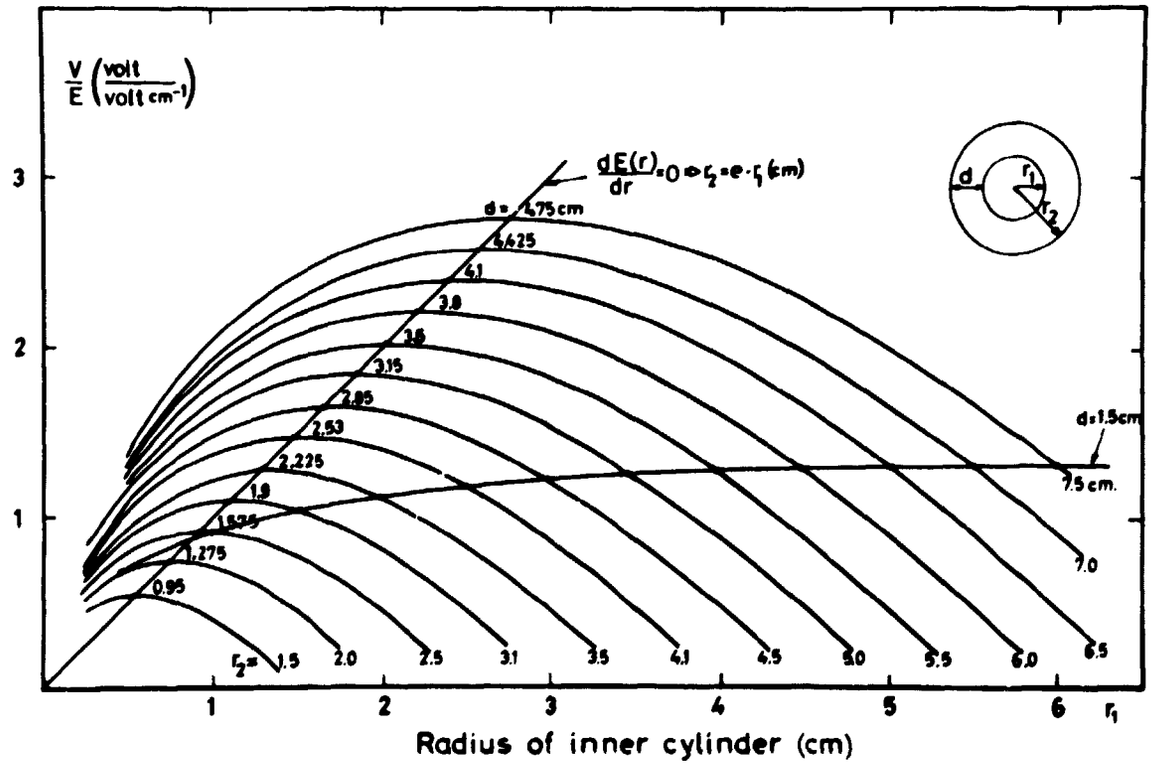

Fig. 7. Potential difference to electric field in coaxial cylinder geometry.

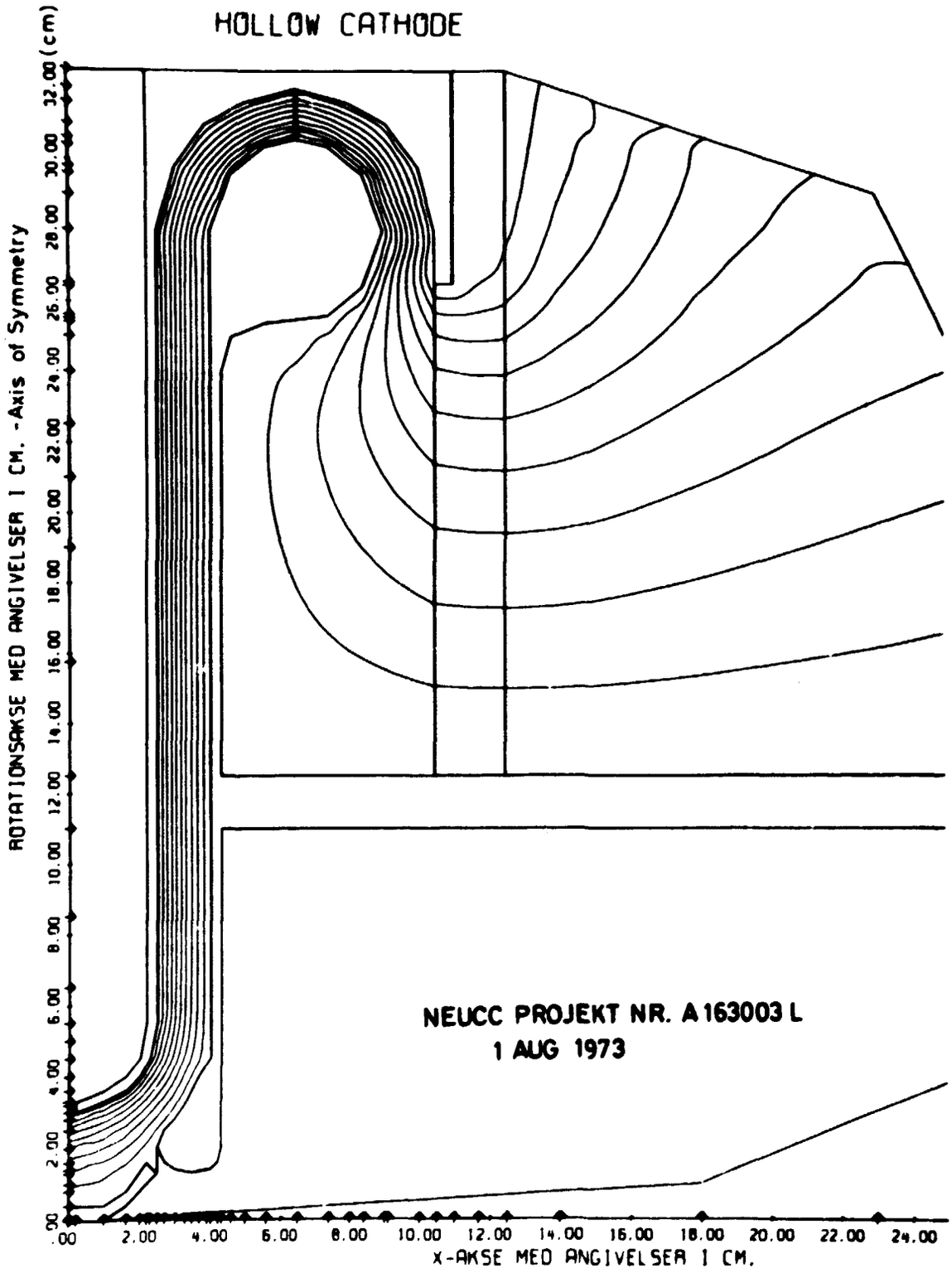

Fig. 8. Computer calculated electric field distribution.

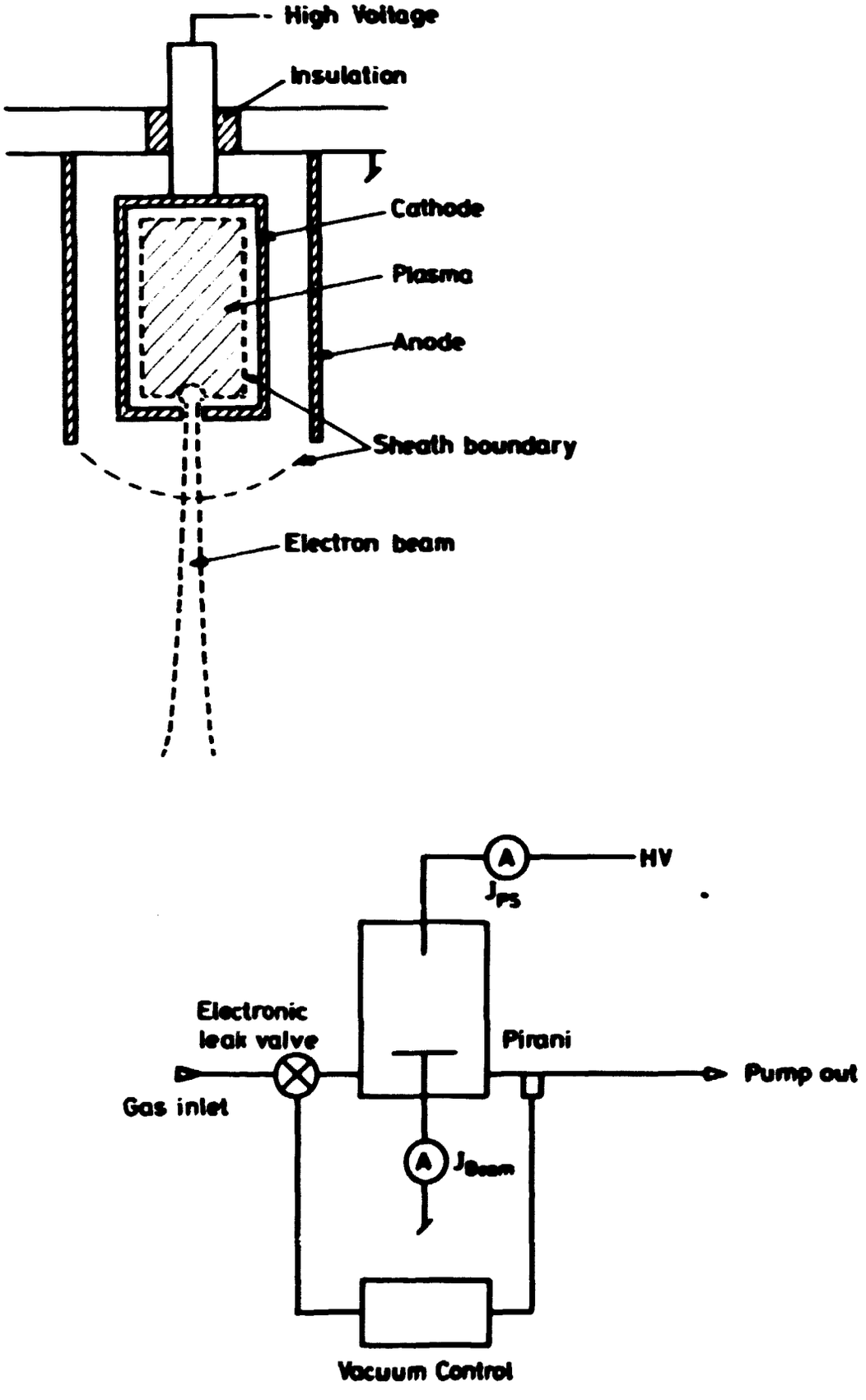

Fig. 9. a) Hollow cathode in principle
b) Hollow cathode set-up, schematically.

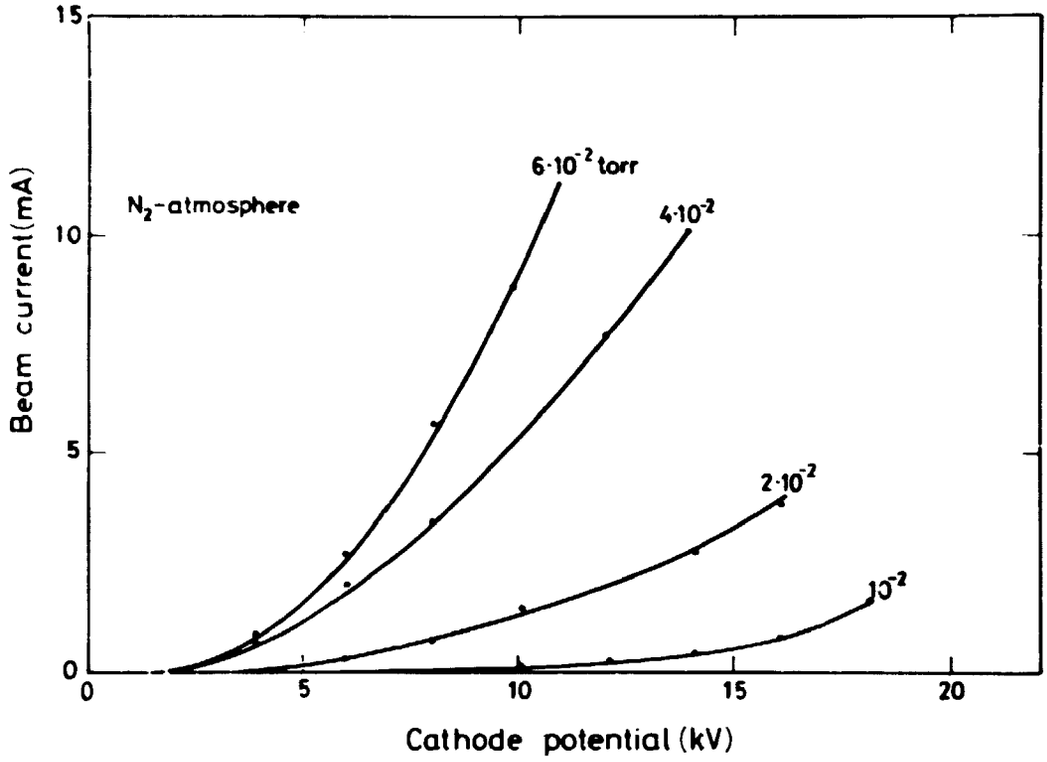

Fig. 10. Beam and power supply current versus cathode potential.

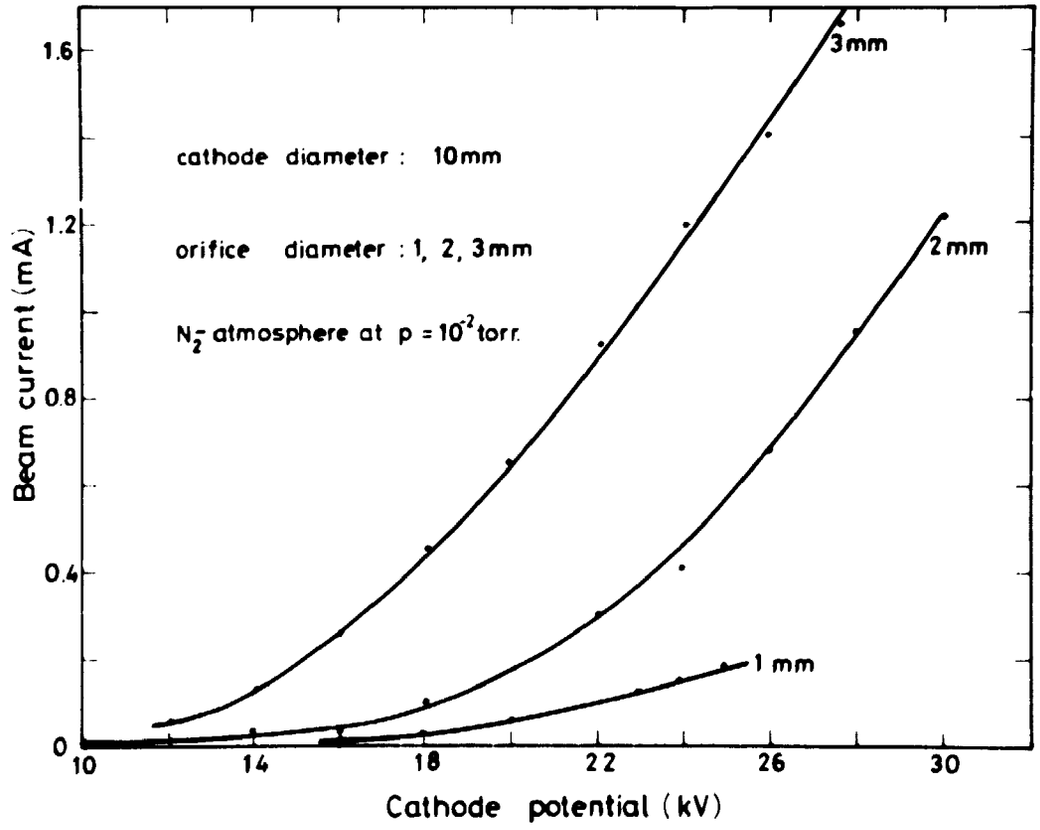

Fig. 11. Beam current and voltage characteristic versus cathode orifice diameter.

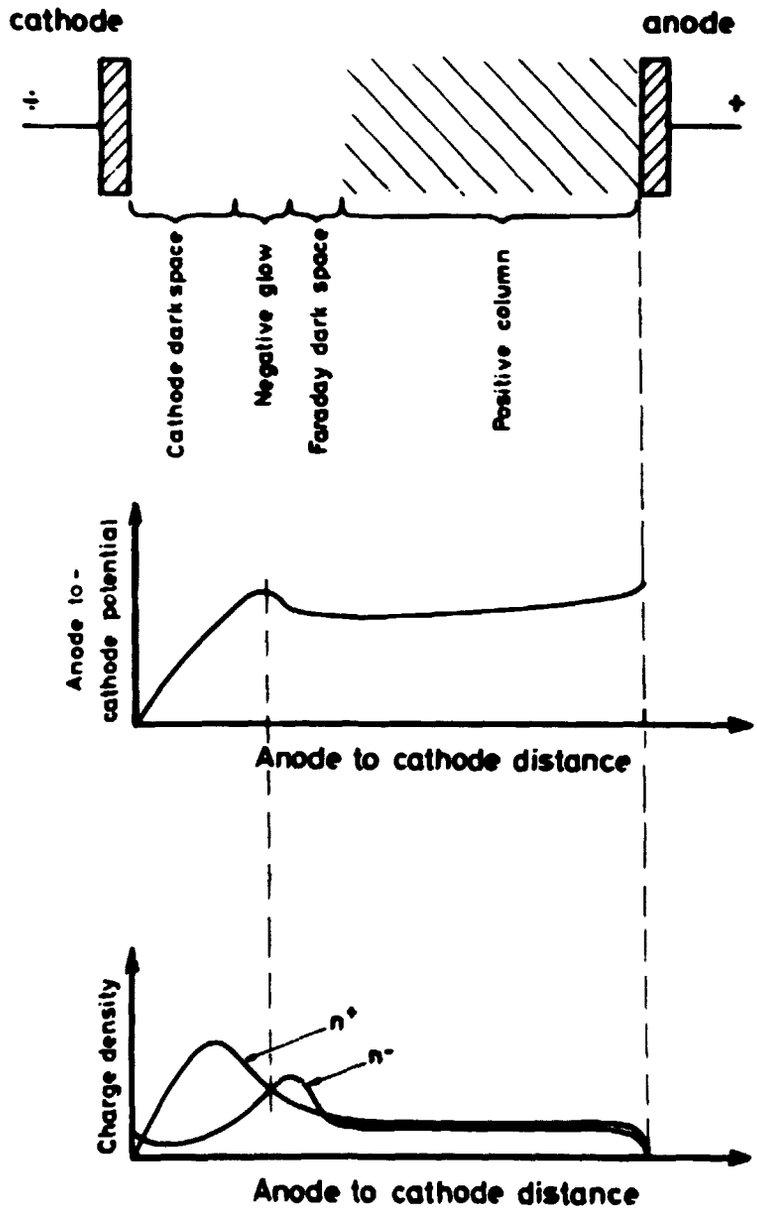

Fig. 12. Glow discharge between parallel plates.

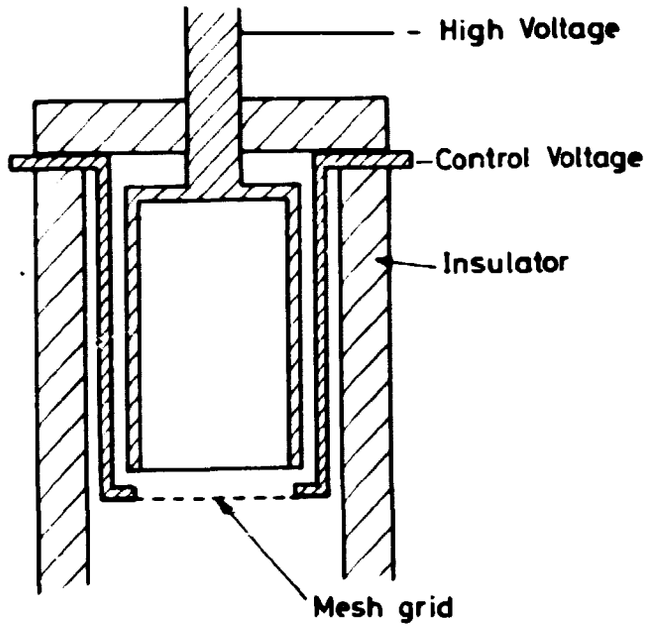

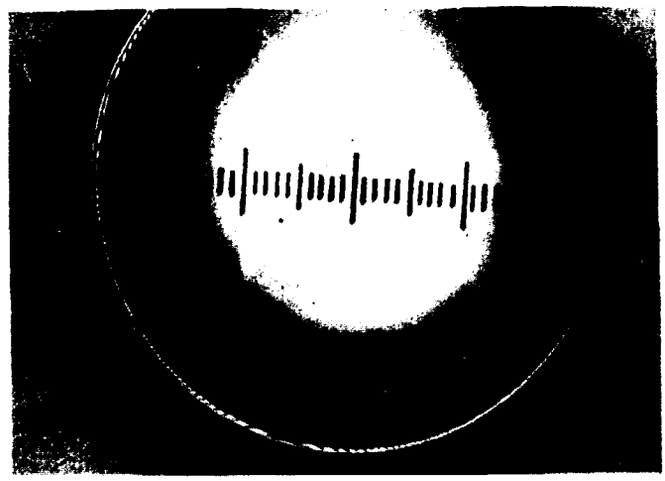

Fig. 13. a) Cathode shown schematically
b) Cathode interior with cathode dark space and plasma column.

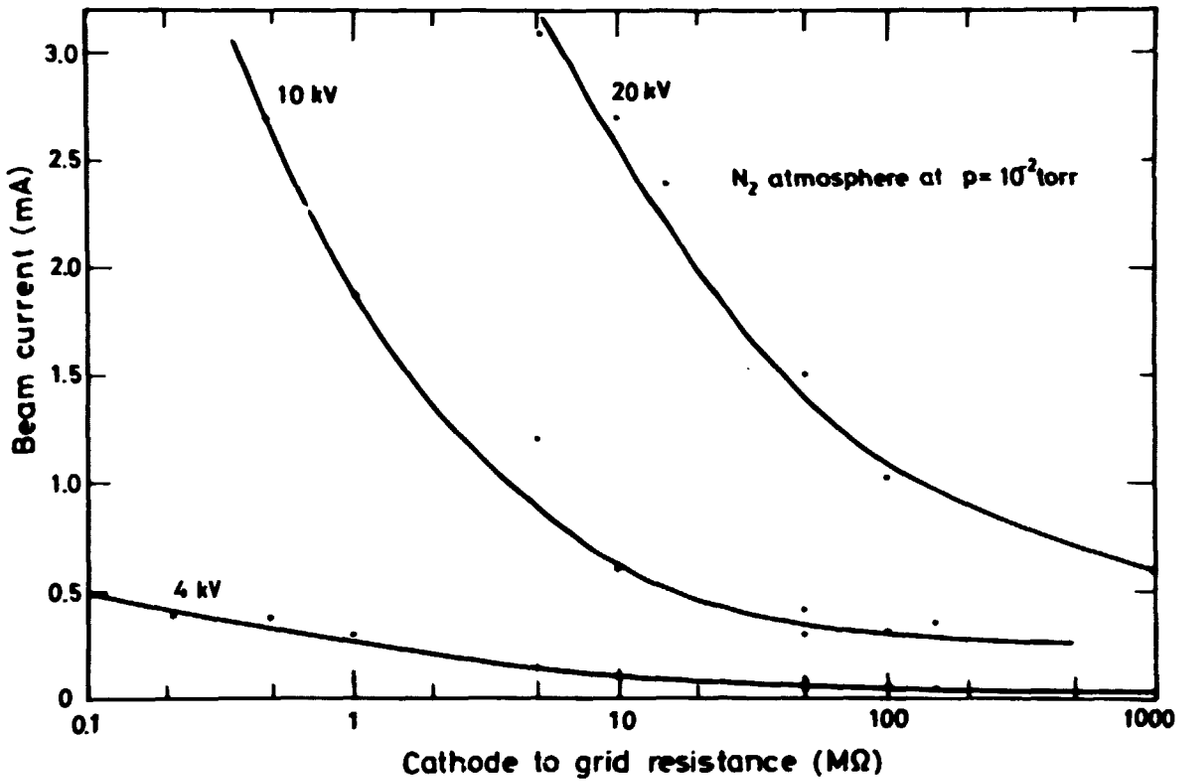

Fig. 14. Beam current as a function of grid to cathode resisteance, cathode high voltage as parameter.

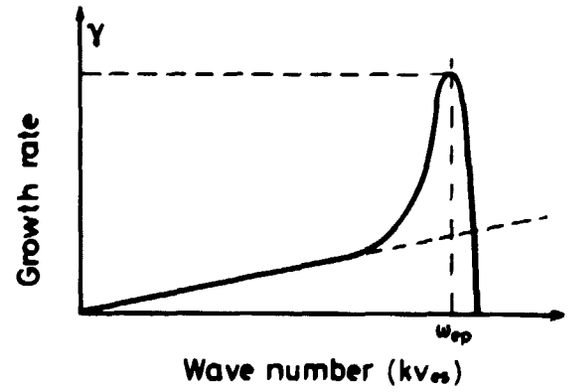

Fig. 16. Temporal growth rate versus the wave number for a weak beam in a plasma, ("Advances in Plasma Physics", Vol. 4 page 57).

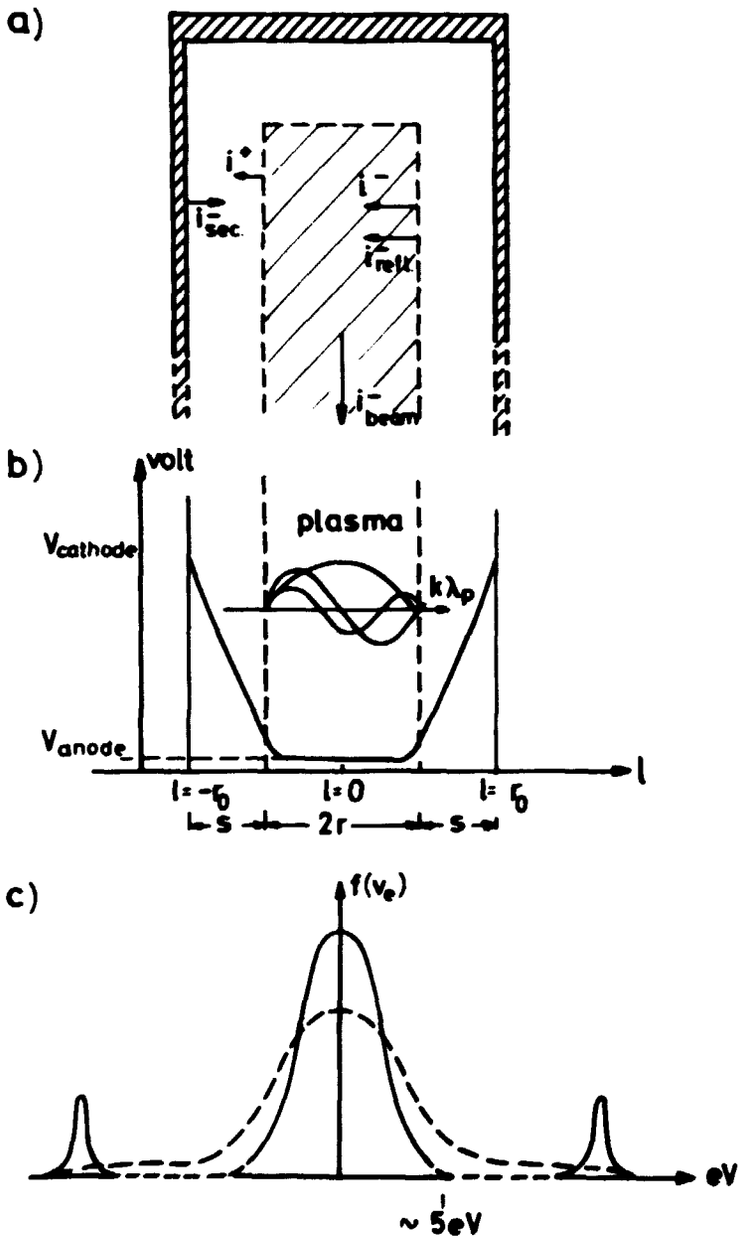

Fig. 15. Schematic representation of a) the main particle currents, b) the potential distribution inside the hollow cathode, and c) the electron velocity distribution before (full line) and after (dotted line) the resonance.

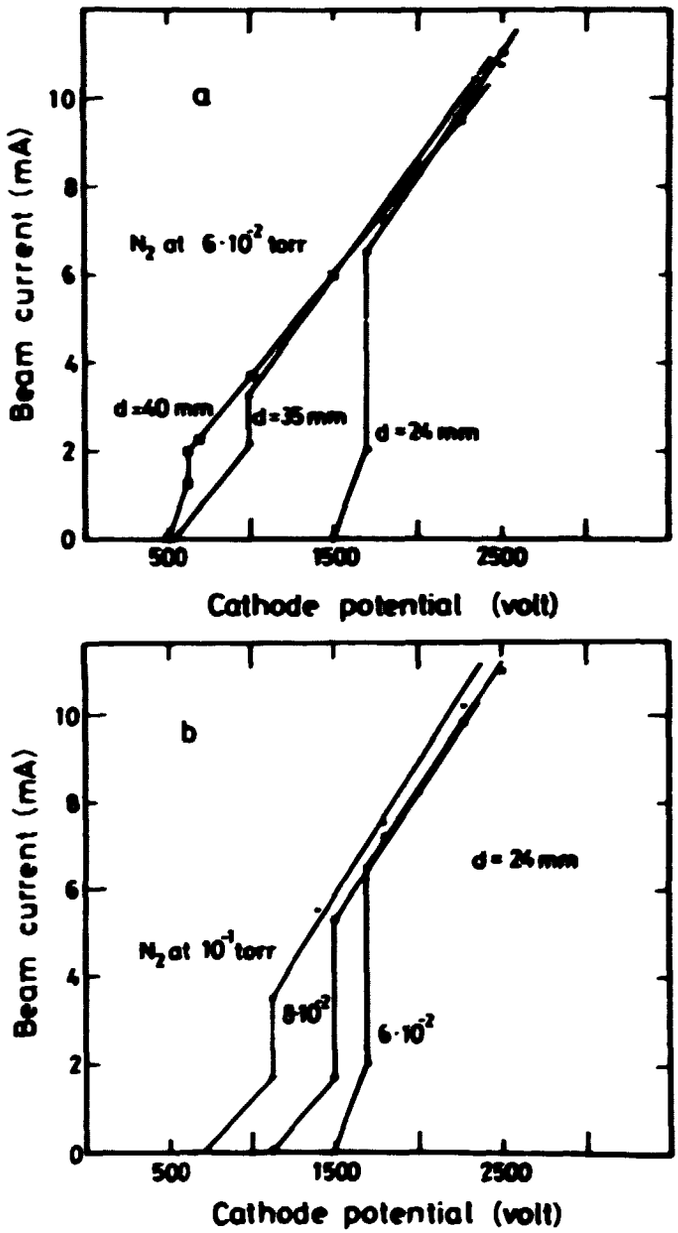

Fig. 17. a) Electron beam current versus cathode potential for different cathode diameters of constant pressure. b) Electron beam current versus cathode potential for different pressures of constant cathode diameter.

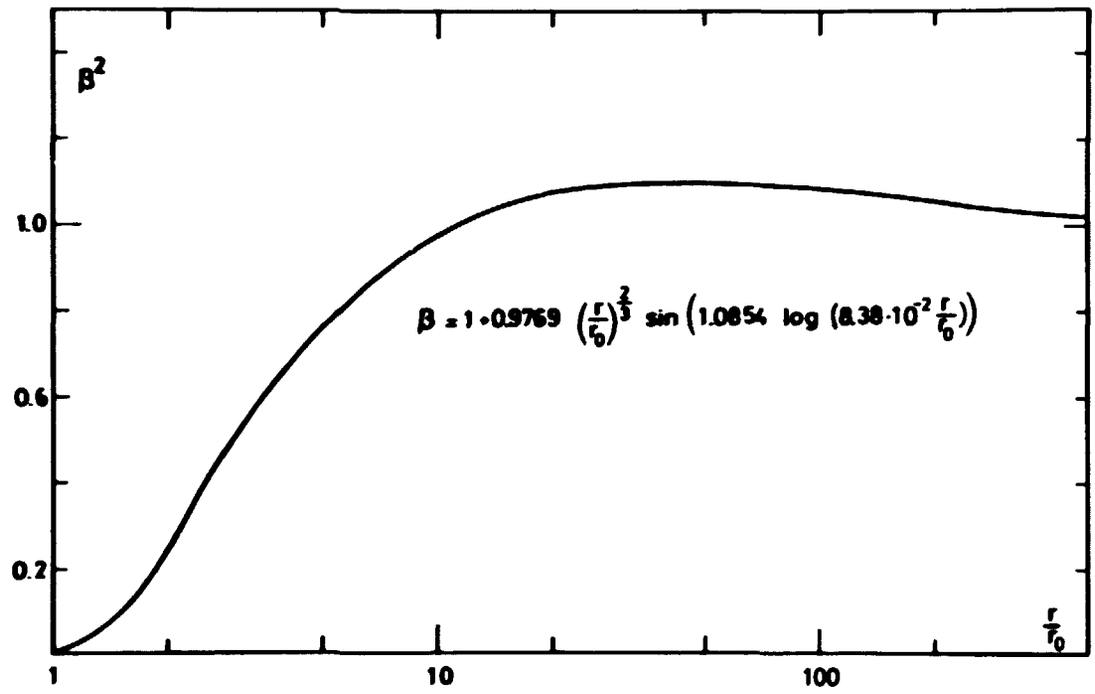

Fig. 18. Geometry factor β^2 as a function of cathode radius to emitting plasma radius $_o$.

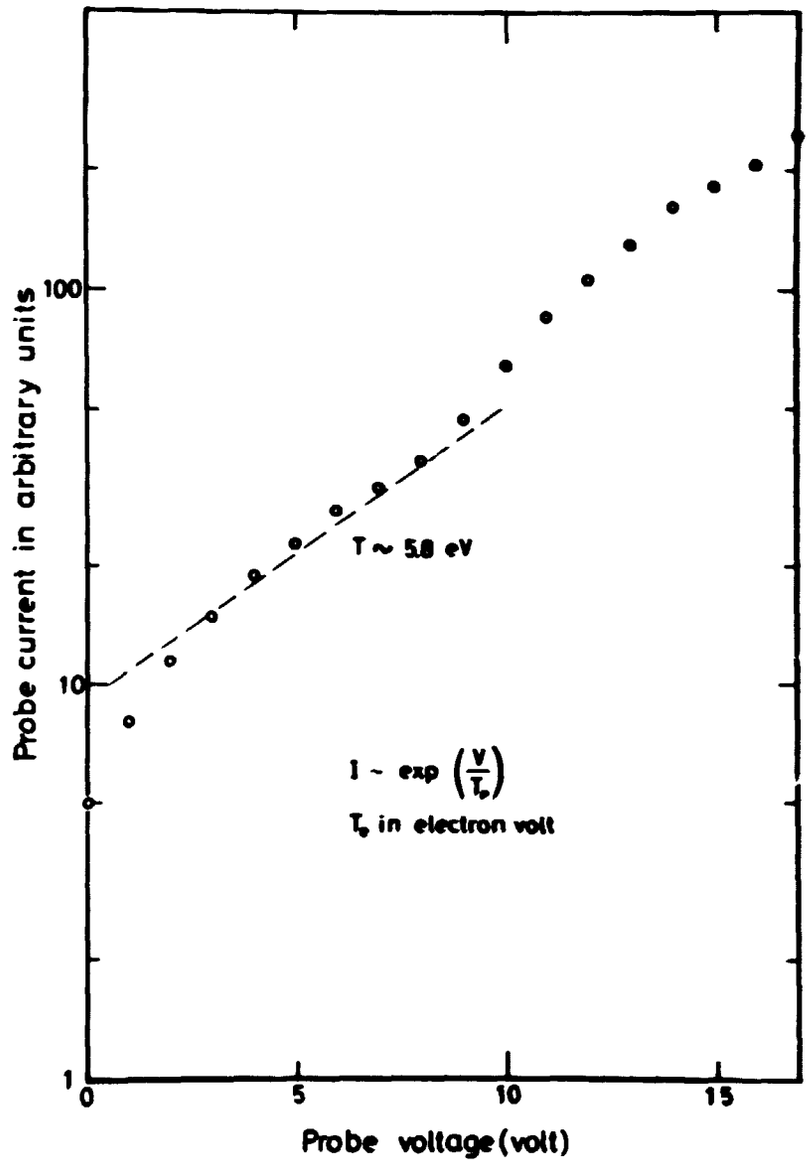

Fig. 19. Electron temperature determined from current-voltage characteristic of a Langmuir probe of area A = $3 \cdot 10^{-7}$ m^2.

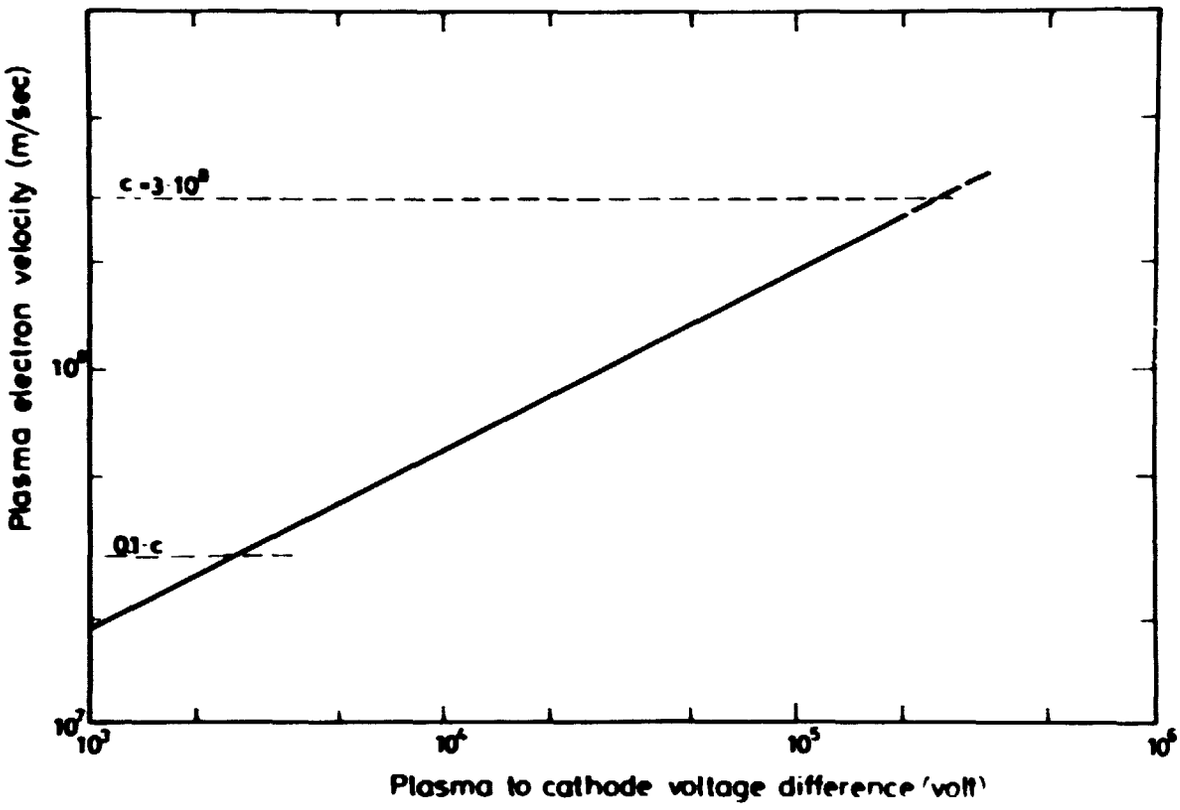

Fig. 20. Plasma electron velocity as a function of the plasma to cathode voltage difference.

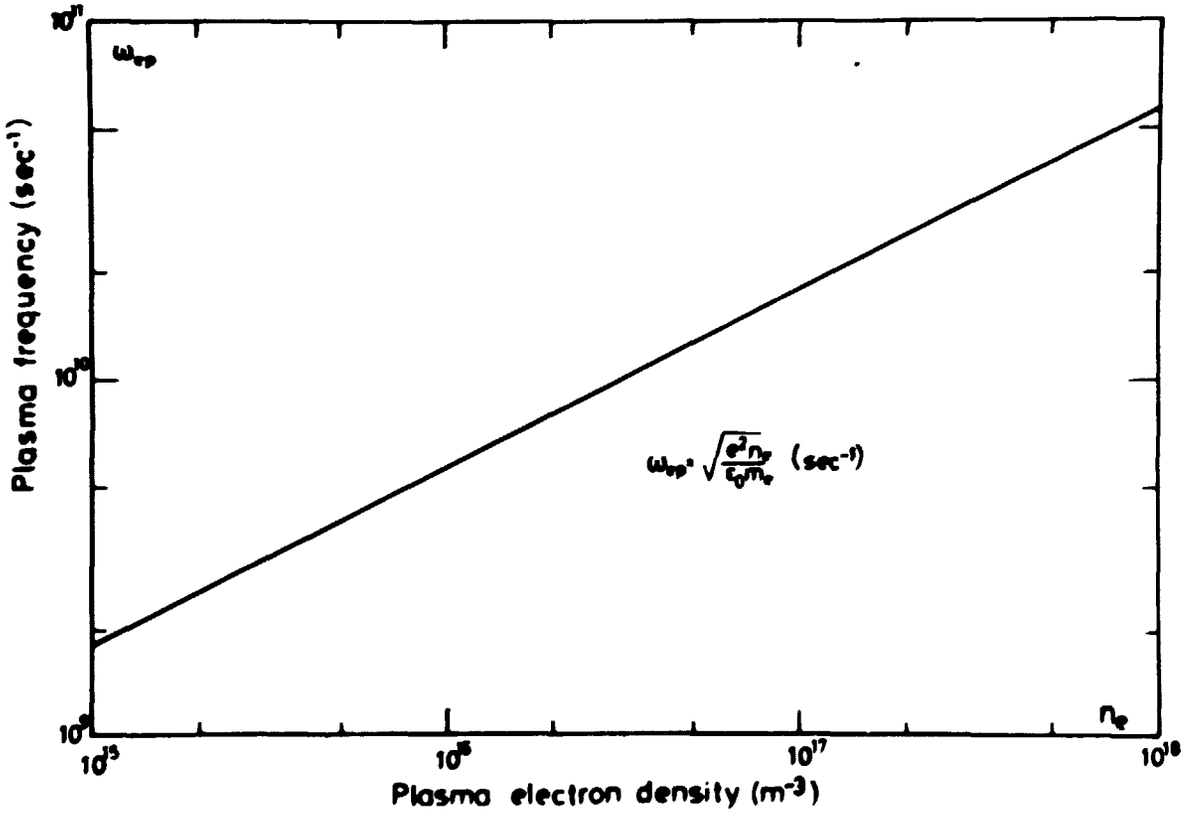

Fig. 21. Plasma frequency as a function of the plasma electron density.

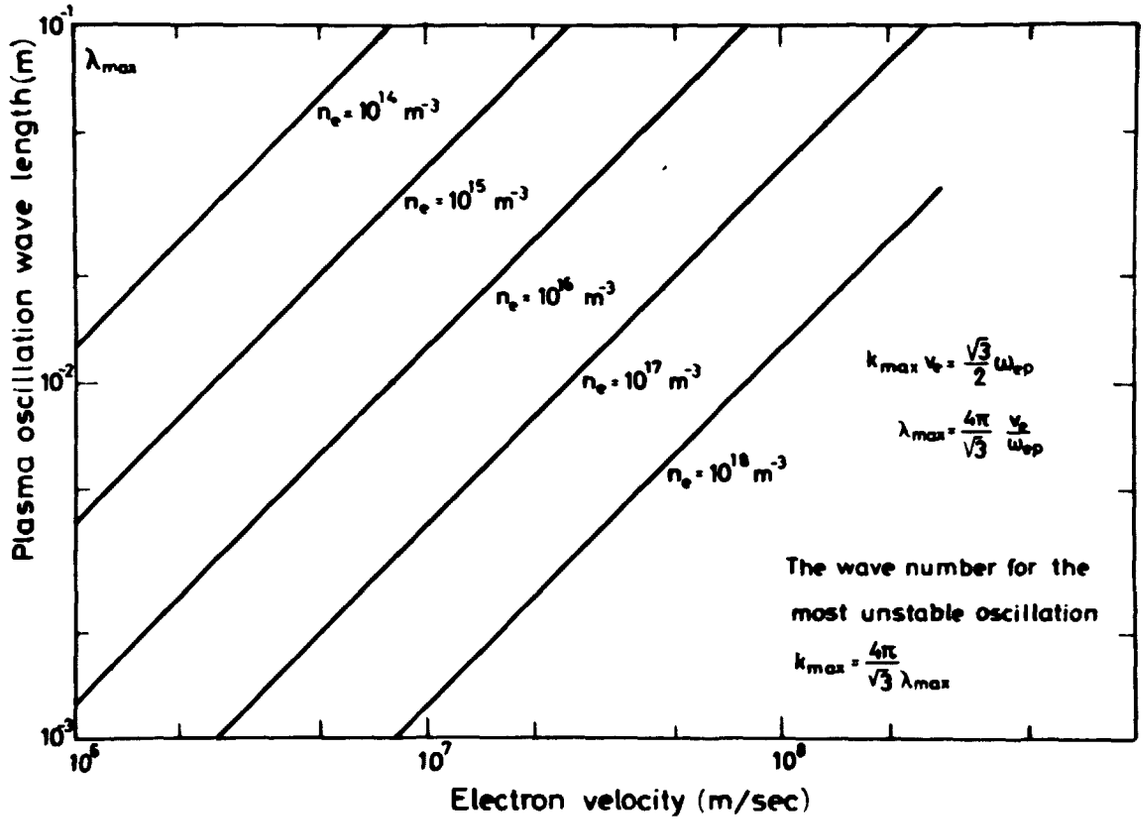

Fig. 22. Plasma oscillation wavelength for the most unstable oscillation as a function of the root mean square thermal velocity of the plasma electrons.

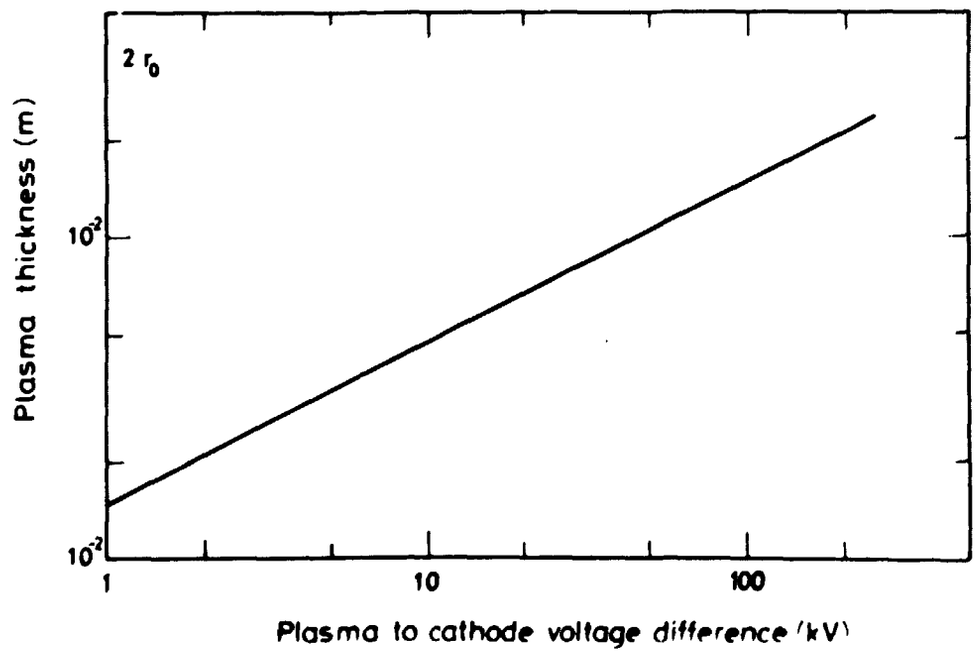

Fig. 23. Optimum plasma thickness as a function of plasma to cathode voltage difference.

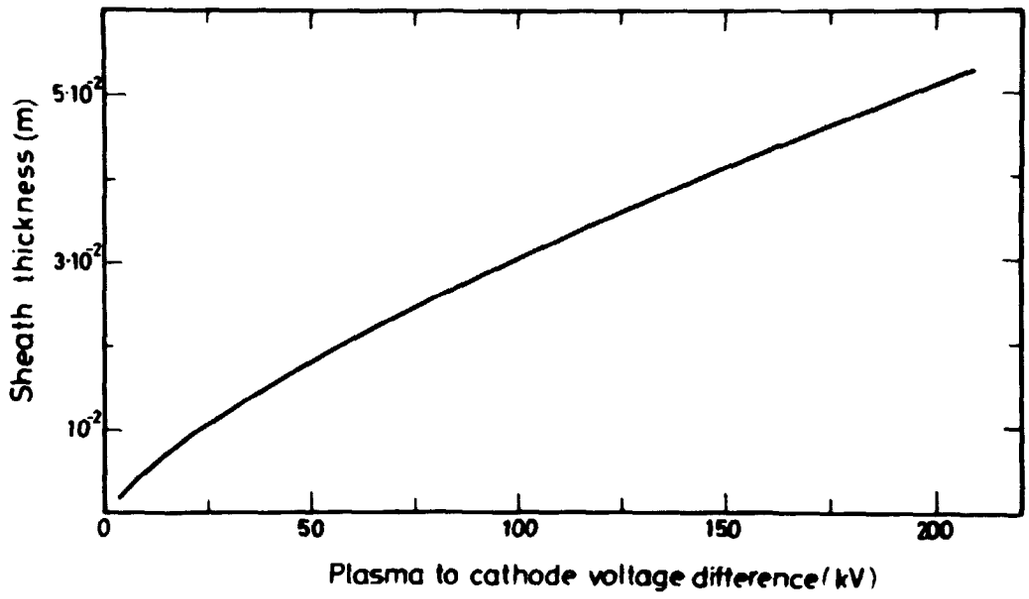

Fig. 24. Calculated sheath thickness as a function of plasma to cathode voltage difference in concentric geometry.

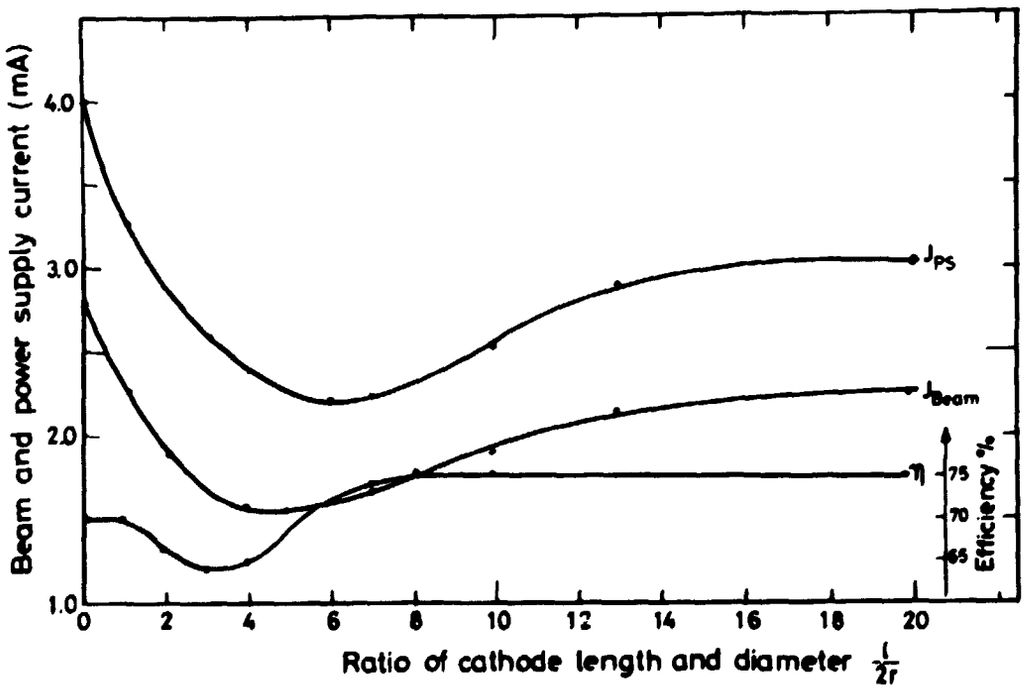

Fig. 25. Beam current, power supply current, and cathode efficiency related to the ratio of cathode cylinder length and diameter at a constant cathode potential of 20 kV.